Journal of *Marine Science and Engineering*

MDPI

Article

Accelerated Warming and Salinification of the Mediterranean Sea: Implications for Dense Water Formation

Nikolaos Skliris [1,*], Robert Marsh [1], Matthew Breedon [1] and Simon A. Josey [2]

[1] School of Ocean and Earth Science, University of Southampton, Southampton SO14 3ZH, UK; r.marsh@soton.ac.uk (R.M.); mattbreedon@gmail.com (M.B.)
[2] National Oceanography Centre, Southampton SO14 3ZH, UK; simon.josey@noc.ac.uk
* Correspondence: n.skliris@soton.ac.uk

Abstract: Trends in the air–sea freshwater and heat fluxes and hydrographic properties of the Mediterranean Sea are investigated to assess changes in dense water formation over 1979–2023 and 2004–2023. Results show a strong annual evaporation increase that has accelerated over the last two decades following the higher warming rate. Positive trends in winter latent heat flux (*LHF*) were obtained over 1979–2023 in most of the East Mediterranean, driving an increase in both the ocean heat loss and the haline component of the surface density flux, but there were no significant long-term trends over the western basin and the dense water formation sites. Results show much larger trends over 2004–2023 when a broadscale decrease in sensible heat flux (*SHF*) is obtained over the western basin as the air temperature is increasing much faster than *SST*. Decreasing (increasing) *LHF* and *SHF* resulted in largely reduced (enhanced) ocean heat loss during winter in the Gulf of Lions (Aegean Sea) over 2004–2023. Robust positive trends are obtained for both the salinity and temperature fields throughout the basin, with accelerated warming and salinification rates after the 2000s. Deep waters have become warmer but also much saltier and denser over recent decades. A water mass transformation method is also used to investigate changes in volumetric distribution in temperature/salinity/density and *T/S* space. Results suggest that salinification over the last 45 years may have strongly enhanced salt preconditioning in all major dense water formation sites, sustaining or even increasing deep water formation despite the increasingly warming climate.

Keywords: Mediterranean Sea; water cycle; heat flux; salinity; temperature; density; water mass transformation; dense water formation

Academic Editor: Chung-yen Kuo

Received: 15 November 2024
Revised: 23 December 2024
Accepted: 25 December 2024
Published: 28 December 2024

Citation: Skliris, N.; Marsh, R.; Breedon, M.; Josey, S.A. Accelerated Warming and Salinification of the Mediterranean Sea: Implications for Dense Water Formation. *J. Mar. Sci. Eng.* **2025**, *13*, 25. https://doi.org/10.3390/jmse13010025

1. Introduction

As a semi-enclosed, highly evaporative sea characterised by a very intense thermohaline (overturning) circulation, the Mediterranean Sea responds drastically to changes in atmospheric forcing, with severe implications for its climate and marine ecosystems. The Mediterranean Sea is indeed considered one of the most prominent and vulnerable climate change "hotspots" [1] as it appears to be changing faster and more dramatically than the global ocean [2], which reached record warmth in 2023 [3]. Especially in the Eastern Mediterranean, surface warming has been accelerating over recent decades, exacerbating sea level rise [4,5] and drying conditions [6,7]. The warming and drying climate of the Mediterranean region over recent decades have resulted in drastic warming and salinification of the whole basin [8–11]. Accelerated warming of the Mediterranean Sea already strongly affects its marine ecosystems with declining oxygen, nutrient content, biomass, and biodiversity [12]. Increased stratification/reduced overturning are expected

to have even stronger implications for both surface and deep marine ecosystems as the upper and deep ocean layers will be more isolated. The Mediterranean Sea is a highly oligotrophic region with oligotrophy increasing eastwards, strongly limiting primary production. Excessive winter mixing, especially encountered in dense water formation sites, allows for sufficient upward nutrient transport into the euphotic layer to sustain primary production, whereas the deep overturning cells supply oxygen from the upper layers to the deep marine ecosystems. Last millennium paleoclimatic reconstructions for the East Med show a persistent warming trend superimposed upon decreased primary production over the last 250 years [13]. A shutting down of the overturning will dramatically increase oligotrophy in the upper layer whilst driving anoxic and hypoxic conditions in the deep layers. Recent excessive ocean upper-layer warming is also already associated with increased intensity and frequency of Mediterranean marine heatwaves and associated extreme weather events [14,15]. A warming-driven increase in stratification is expected to further accelerate the warming rate of the upper ocean layer as it will gradually be more isolated from the deep ocean, accentuating marine heatwaves and associated extreme weather events in the near future.

Inflowing low-salinity Atlantic Water (AW) is transformed into very saline Mediterranean intermediate and deep waters under strong net evaporation. The density contrast between the high-salinity Mediterranean water and the low-salinity AW drives an inverse estuarine circulation with Mediterranean denser water exiting through the Gibraltar Strait into the Atlantic Ocean, below the AW layer, to balance the net evaporation over the Mediterranean Sea surface. The southeastern Levantine Basin is the location of Levantine Surface Water (LSW), one of the highest-salinity surface water masses in the world's oceans, which is formed under excessive evaporation. LSW typically feeds the Rhodes Gyre (Figure 1) with very salty waters, strongly preconditioning the formation of Levantine Intermediate Water (LIW). Cretan Intermediate Water (CIW), another intermediate salty water mass similar to LIW but produced in the Cretan Sea, is also strongly preconditioned by LSW [16,17]. LIW and similar types of intermediate salty waters, in turn, act as a "thermohaline engine" that drives the upper thermohaline conveyor belt of the whole Mediterranean.

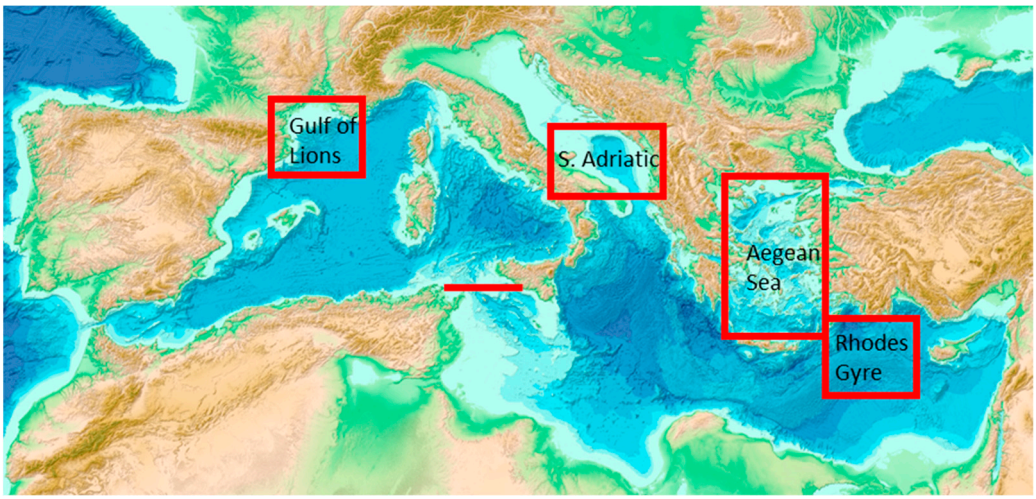

Figure 1. Bathymetry map of the Mediterranean Sea (General Bathymetric Chart of the Oceans (GEBCO), https://download.gebco.net/ (accessed on 22 December 2024). The four major dense (intermediate/deep) water formation areas, i.e., Aegean Sea, Rhodes Gyre, South Adriatic Sea, and Gulf of Lions, are also depicted by red boxes. The red zonal section across the Sicily Strait delimiting WMED and EMED sub-basins is also depicted.

LIW enhances salt preconditioning and plays an important role in controlling deep water formation via open ocean convection during winter, although variations in air–sea heat flux-driven buoyancy loss are likely the primary control [18]. The three major deep water formation sites of the basin (Figure 1) are the Aegean Sea and South Adriatic in the East Mediterranean (EMED), where Cretan Deep Water (CDW), North Aegean Deep Water (NAeDW), and Adriatic Deep Water (ADW) contribute to the bulk of East Mediterranean Deep Water (EMDW); the Gulf of Lions in the West Mediterranean (WMED) is the major contributor to West Mediterranean Deep Water (WMDW). A detailed description of all major water masses and their involvement in the Mediterranean overturning circulation may be found in [19]. LIW fills large parts of the Mediterranean basin in an approximate depth range of 150–600 m, identifiable by a subsurface salinity maximum, with a portion of it eventually overflowing the sill at the Strait of Gibraltar. In addition, very dense water may also be formed by shelf cascading in both the North Aegean [20,21] and NW Mediterranean [22], occasionally contributing to the bulk of EMDW and WMDW, respectively. Therefore, the Mediterranean overturning circulation may be seen as primarily comprised of a zonal overturning cell driven by LIW circulation across the whole basin and two meridional overturning cells driven by deep water formation in each sub-basin [19,23].

LSW salinity has been strongly increased since the mid-1960s due to a dramatic reduction of river freshwater inputs after the damming of major rivers (the Nile River in particular) and increasingly drier conditions in the Levantine Basin [24]. A strongly increasing salinity signal of LIW is now observed throughout the whole basin [8,10,25], and it is even evidenced in the Mediterranean Overflow Water (MOW) exiting through the Gibraltar Strait into the subtropical Northeast Atlantic at ~1000 m [26], with implications for the stability/intensity of the Atlantic Meridional Overturning Circulation (AMOC) [27–29].

Although ocean stratification has substantially increased globally over the last few decades mainly due to the excessive warming of the upper layer [30], there are no significant changes in the vertical stratification of the Mediterranean upper water column as salinification and warming trends are shown to be almost density compensated over the second half of the 20th century [26]. However, hydrographic campaigns in the 1990s and 2000s evidenced sudden abrupt climatic transient events of the Mediterranean overturning circulation under anomalously strong winter cooling episodes and salt preconditioning, i.e., the so-called East Mediterranean Transient (EMT, 1987–1994) [31–33] and Western Mediterranean Transition (WMT, 2005–2010) [9,34], respectively, with excessive dense water formation taking place over a few years resulting in warmer, more saline, and denser waters in the deep layers of both sub-basins. In particular, during the EMT, the deep water formation rate in the Aegean Sea (which replaced the S. Adriatic as the major source of EMDW) was estimated to be an order of magnitude larger than that observed before [35]. Increased LIW salinity signal from EMT travelled to the western basin and probably resulted in enhanced salt preconditioning, facilitating larger deep water formation in the Gulf of Lions during the WMT [36,37]). Long-term large warming and salinification of the intermediate and deep layers were observed throughout the western basin [8,9], as well as in the MOW at the Gibraltar Strait [38] and in the subtropical North Atlantic [39].

More recent observational studies covering the last 15 years still indicate a very active circulation of saltier/warmer LIW and similar types of East Mediterranean intermediate waters such as Cretan Intermediate Water (CIW) across the eastern basin [16,17,20,21,40,41], sustaining sporadic deep water formation in the East Mediterranean formation sites. In particular, a very abrupt shift of increasing temperature and salinity of LIW was observed in 2007 within the East Levantine Basin [42]. Since 2015, the South Adriatic Pit has registered a strong increase in salinity at intermediate layers, a deepening of the mixed layer and an increasing density of the deep layer [40,43]. Salt preconditioning seems to be still

very efficient in sustaining intermediate/deep water formation in the Aegean Sea with significant but weaker EMT-type events over the last 15 years [16,20,21,44]. In particular, the Aegean Sea has shown excessive salinification at intermediate layers since 2019, and it is in a state of increased dense water formation due to the combination of increased surface buoyancy loss and reduced Black Sea Water (BSW) inflow, although intense upper layer warming seems to prevent widespread formation of denser waters [21]. Significant abrupt increases in salinity and density of deep waters are observed around the western basin after the mid-2000s [8,9]. However, there has not been any significant deep water formation in the Gulf of Lions over the last decade despite the observed salinity increase at intermediate layers within the western basin [18,45].

The Med-CORDEX ensemble 21st-century projections (six regional climate models; three RCP scenarios) show that Mediterranean water masses will continue to become saltier and warmer but less dense during the 21st century [46]. There is a climate model consensus that the intensity of the deep water formation in the Gulf of Lions will be largely decreased by the end of the century; however, the rate of decrease remains very uncertain depending on the greenhouse gas emissions scenario and climate model chosen. There is no model consensus concerning the change in the intensity of deep water formation in the Adriatic Sea and in the Aegean Sea, although most models also point to a reduction [46]. However, more recent, higher resolution regional climate model simulations under the high-emission scenario (RCP8.5) show more dramatic changes in the overturning circulation with an early collapse of deep water formation in the Gulf of Lions by mid-century [47], which observations indicate is already underway [18,45]. Furthermore, there will be a large reduction in deep water formation at all EMED formation sites by the end of the century [48]. Therefore, two key research questions arise regarding the present and future status of the Mediterranean overturning circulation: (a) How effective is the salt preconditioning for deep water formation, both currently and in the future, in the two sub-basins as surface and intermediate water masses become saltier and warmer under an increasingly drier and warmer regional climate? (b) Is there a permanent eastward shift in the locus of Mediterranean deep water formation towards the eastern basin and the Aegean and South Adriatic Seas, in particular, as suggested by Josey and Schroeder [18]?

The aim of this study is to investigate the long-term trends in air–sea freshwater and heat fluxes and their impact on hydrographic properties of the Mediterranean basin using atmospheric reanalysis and ocean observationally based datasets. Air–sea flux datasets are used to calculate surface density fluxes and their trends controlling dense water formation. Two periods are considered for trend analysis: the long-term 1979–2023 period and the most recent 20-year period (2004–2023), when significantly more substantial changes were obtained in air–sea fluxes and hydrographic properties. A water mass transformation method is also applied to quantify changes in volumetric distributions in salinity (S), temperature (T), density (σ_0), as well as T/S space to assess changing characteristics and transformation rates of the major Mediterranean water masses over 1979–2023. The main focus is on changing surface haline/thermal density fluxes, hydrographic properties, and water mass transformation rates in the major dense (intermediate and deep) water formation areas over wintertime that control the intensity of the zonal and meridional overturning circulation cells of the Mediterranean basin [19,23].

2. Material and Methods

This study rests on the use of the most recent state-of-the-art hydrological/air–sea flux global gridded datasets covering the period 1979–2023. We consider a shorter period than the 70-year span, 1951–2020, employed by Josey and Schroeder [18] in their air–sea flux analysis in order to make use of in situ ocean temperature and salinity datasets that have

richer coverage in the recent decades, as well as better constrained reanalysis outputs with assimilation of satellite-derived *SST* which begins in the early 1980s.

The ECMWF ERA5 reanalysis dataset [49] is used to provide high-resolution (0.25° longitude/latitude grid) monthly air–sea flux data (downloaded from the Copernicus Marine Service, https://cds.climate.copernicus.eu/datasets/reanalysis-era5-single-levels-monthly-means?tab=overview (accessed on 25 March 2024). Specifically, we analysed monthly Evaporation, Precipitation, Air Temperature at 2 m, *SST*, Net Shortwave Radiation (*NSWR*), Net Longwave Radiation (*NLWR*), Latent Heat Flux (*LHF*), and Sensible Heat Flux (*SHF*). The sign convention for heat fluxes used for the surface heat budget was as follows:

Total net heat flux (to the ocean) (*NHF*) = *NSWR* (to the ocean)—*NLWR* (to the atmosphere)—*LHF* (to the atmosphere)—*SWF* (to the atmosphere), whereby, during winter, total *NHF* is negative (positive to the atmosphere) as *LHF* + *SHF* + *NLWR* > *NSWR*, which is equivalent to ocean net heat loss (*NHL*) (to the atmosphere), which is used hereafter.

The UK Met Office Hadley Centre Enhanced Ocean Data Assimilation and Climate Prediction (ENACT), archive version 4 (EN4, subversion En4.2.2 (En4.2.2.g10.analyses), http://www.metoffice.gov.uk/hadobs/en4 (accessed on 25 March 2024)), is used here to provide objectively analysed gridded monthly 3-D salinity and temperature data (1 degree horizontal grid, 42 depth levels). The starting year for all datasets was set to 1979 as atmospheric reanalysis is better constrained by satellite-derived data, and coverage of in situ salinity/temperature observations is also greatly enhanced.

The high-resolution (0.25° horizontal grid) NOAA Optimal Interpolated Sea Surface Temperature (OISST, version 2) monthly dataset (https://psl.noaa.gov/data/gridded/data.noaa.oisst.v2.highres.html (accessed on 25 March 2024) is also used, based on a combination of ocean temperature observations from satellite and in situ platforms, available for the period 1982–2023, to compare with ERA5 *SST* trends in the Mediterranean Sea.

The total surface density flux (i.e., the equivalent of negative surface buoyancy flux) is derived from ERA5 monthly air–sea heat/freshwater flux datasets at each grid point. The surface thermal density flux D_T and surface haline density flux D_S were calculated as follows:

$$D_T = -\frac{\alpha(T,S)}{C_p} NHF \text{ in kg m}^{-2}\text{ s}^{-1} \quad (1)$$

$$D_S = -\rho_0 \beta(T,S) \frac{\left(\frac{SSS}{1000}\right)}{1-\left(\frac{SSS}{1000}\right)} FWF \text{ in kg m}^{-2}\text{ s}^{-1} \quad (2)$$

where $\alpha(T,S) = -\frac{1}{\rho_0}\frac{\partial \sigma}{\partial T}\Big|_{T,S}$ is the thermal expansion coefficient ($^\circ\text{C}^{-1}$).

$\beta(T,S) = \frac{1}{\rho_0}\frac{\partial \sigma}{\partial S}\Big|_{T,S}$ is the haline contraction coefficient (dimensionless).

C_p is the specific heat capacity of seawater (J kg^{-1} $^\circ$C^{-1}).

NHF is the surface net heat flux to the ocean (Wm^{-2}).

ρ_0 is the representative density for seawater (1025 kg m^{-3}).

FWF is the surface net freshwater flux ($P + R - E$) (in m s^{-1}).

SST ($^\circ$C) and SSS (pss) are the sea surface temperature and salinity, respectively.

The total surface density flux, D_{TOT}, is the sum of the thermal and haline surface density flux terms, $D_{TOT} = D_T + D_S$, $\left(\text{kg m}^{-2}\text{ s}^{-1}\right)$.

Annual and winter mean timeseries are produced for all variables. Winter is defined here as January–February–March, which is the typical period for dense (intermediate and deep) water formation in the Mediterranean Sea [23]. Linear trends have been computed by least square fitting for periods 1979–2023 and 2004–2023, and trend errors are defined at 95% confidence intervals. The p-value for statistical significance of a correlation coefficient between two timeseries is computed by transforming the correlation to create a t-statistic

with N-2 degrees of freedom, where N is the number of data points in the timeseries. Area-averaged timeseries are produced for the four main dense water mass formation areas, as well as EMED and WMED sub-basins delimited by a zonal section at the Sicily Strait (see Figure 1).

In order to assess freshwater transformation in the Mediterranean basin under the changing water cycle, we used a thermodynamic method developed by Zika et al. [50] and applied it to the analysis of the Mediterranean freshwater budget [24] based on the water mass transformation theory [51]. The movement of an individual water parcel in salinity coordinates is given by the following equation:

$$\frac{DS}{Dt} = S_o(E - P - R) + \nabla.K\nabla S \quad (3)$$

where S_o is the volume-averaged mean salinity, and K is a positive definite diffusion tensor. A water parcel changes its salinity, S, through surface freshwater flux ($E - P - R$) and salt mixing. Considering the volume of seawater bound by the isohaline $S = S^*$, given by $V(S^*) = \iiint_{S<S*} dxdydz$, the total movement of freshwater across an isohaline surface is given by integrating both RHS terms of Equation (3):

$$MTR(S) = \frac{dV(S^*)}{dt} = \iiint_{S<S^*} \delta\left(S - S^*\right)(S_o FWF - \nabla.K\nabla S)dxdydz, \quad (4)$$

where δ is a Dirac delta function.

Equation (4) states that the rate of change in the volume of water, $MTR(S) = dV(S)/dt$, i.e., the water mass transformation rate in salinity space, is set by the water cycle (i.e., the net air–sea freshwater flux to the ocean, $FWF = P + R\text{-}E$) and interior salt mixing across isohaline surfaces. A positive rate denotes a transformation from saline to fresh water, and a negative rate denotes a transformation from fresh to saline water. At global scale, the water cycle broadens the volumetric distribution in salinity coordinates (increasing the volumetric freshwater displacement) as the salinity contrast increases and, on the contrary, salt mixing tends to collapse the volumetric distribution as it always takes salt from the more saline waters and mixes it with the less saline waters [50,52]. In a warming climate, the global water cycle is amplified, leading to an increase in volumetric freshwater displacement from more saline to less saline waters (fresh waters become fresher, salty waters become saltier), while at the same time, the mixing term also increases, partially counterbalancing the amplification of the water cycle. If we ignore the salt mixing term in Equation (4), the integral of MTR in salinity space (L.H.S of Equation (4)) provides an estimate of the change of the water cycle amplitude [50,53]. In regions of net evaporation, such as the Mediterranean Sea, a negative (positive) value of the MTR integral in salinity space denotes the total increase (decrease) of net evaporation, i.e., the total accumulated freshwater volume removed from (gained by) the basin. Skliris et al. [24] demonstrated that the relative contribution of the salt mixing term is very small (~5%) and not statistically significant compared to the water cycle term (net evaporation increase) in producing the observed pronounced change in the Mediterranean volumetric distribution in salinity space over the last five decades. Therefore, we may assume that the water mass transformation rates obtained here are predominantly due to net evaporation change.

Equation (4) generally stands for an enclosed system, i.e., the global ocean or an enclosed oceanic basin. In the case of a semi-enclosed basin, such as the Mediterranean Sea or a region with open lateral boundaries, the RHS term of Equation (4) should also include the freshwater displacement due to changes in the transports at the straits or open boundaries. The distribution of water mass transformation can give us important insights into where and by how much important water masses with distinct salinity signatures

are transformed over the considered period. Here, we use EN4 3-D monthly data to estimate water mass transformation rates. First, we calculate the salinity linear trend over 1979–2023 at each grid point of the Mediterranean Sea volume. Then, based on the linear trends, we calculate the total change in volumetric distribution in salinity coordinates over 1979–2023 to estimate long-term water mass transformation rates. For more details regarding the application of this method to the Mediterranean Sea freshwater budget change, see Skliris et al. [24].

As the water mass transformation theory applies in spaces of all conservative tracers [54], we used the same approach to also calculate mass transformation rates in temperature ($dV(T)/dt$) and density ($dV(\rho)/dt$) coordinates, based again on the long-term 3-D temperature and density trends (from En4) and the respective volumetric distribution changes. Volumetric change in temperature space occurs via net surface heat flux and interior cross-isothermal mixing, and volumetric change in density space occurs via total (haline + thermal) surface density flux and cross-isopycnal mixing.

Finally, we also calculated changes in volumetric distributions to assess water mass transformation in *T/S* space (i.e., $dV(T,S)/dt$), the natural space of water masses, to better understand regional transformations of major Mediterranean surface, intermediate, and deep water masses over 1979–2023. Transformation rates are defined here as volumetric fluxes of water in and out of *T/S* classes based on the *T/S* linear trends over the 1979–2023 period.

3. Results

3.1. Air–Sea Fluxes

3.1.1. Freshwater Flux and *SST* Trends

Figure 2 illustrates spatial patterns of trends in annual mean *E*, *P*, *E-P*, and *SST* over 1979–2023. Results show long-term widespread surface warming and evaporation increases across the basin (Figure 2a). The annual *SST* trend averaged over the whole Mediterranean surface is 0.31 °C per decade over 1979–2023 (~1.4 °C per 45 years), whilst surface warming has accelerated over the last two decades at 0.45 °C per decade. Evaporation and *SST* trend patterns are quite similar. Positive evaporation trends over 1979–2023 are stronger in the Levantine Basin (>0.3 m year^{-1} per 45 years), which is consistent with excessive SST warming trends, exceeding 1.7 °C per 45 yrs (Figure 2d). It is interesting to note there are much lower warming (<1 °C per 45 years) and evaporation trends (<0.1 m year^{-1} per 45 years) along the AW pathway compared to surrounding Mediterranean waters in the western basin. The correlation coefficient between the annual timeseries of the two variables exceeds 0.6 in most of the regions. Previous studies have also shown increasing latent heat of evaporation associated with increased surface warming in the Mediterranean surface, suggesting that evaporation increases were at least partially driven by surface warming [24,55–57]. In contrast with evaporation, the precipitation trend pattern shows much lower, less coherent, and mostly not statistically significant trends over this period. The pattern is characterised by large spatial variability with predominantly decreasing precipitation values in the southern part of the basin and increasing precipitation values in central/northern parts, notably in the Southern Adriatic/North Ionian, North Aegean, and East Tyrrhenian Seas. The *E-P* trend pattern is largely driven by evaporation increases. Especially in *EMED*, south of 37 °N, there is a coherent broadscale net evaporation increase across the basin. In contrast, in the Adriatic/N. Ionian and North Aegean Seas, no significant *E-P* trend is obtained, as the increase in *P* largely counterbalances the increase in *E*.

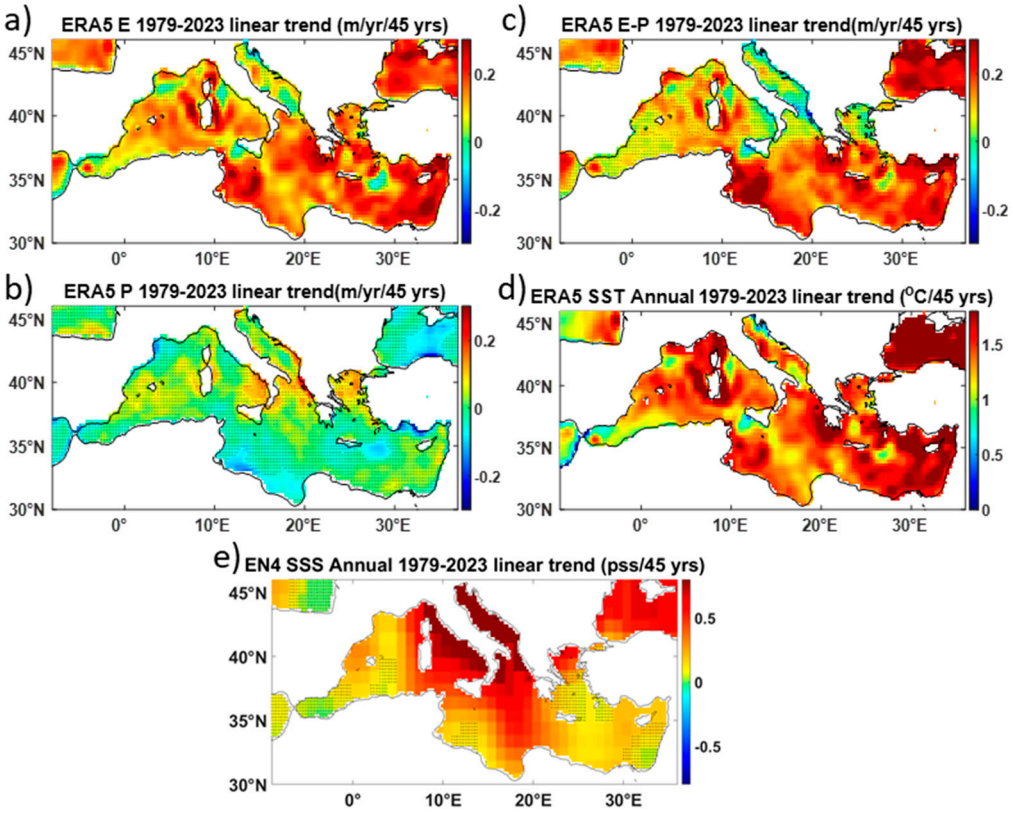

Figure 2. Spatial patterns of linear trends (1979–2023) in annual mean *E* (**a**), *P* (**b**), *E–P* (**c**), (m year^{-1} per 45 years *SST* (°C per 45 years) (**d**) (from ERA5 reanalysis), and *SSS* (pss per 45 years) (from En4) (**e**). Regions where the linear trend is not statistically significant at the 95% confidence interval are stippled.

Area-averaged annual timeseries show strong interannual variability but with increasing positive anomalies in *E* driving larger *E-P* increases after the late 1990s following the acceleration of the warming rate (Figure 3). Results are consistent with previous studies showing increasing annual latent heat loss/evaporation over the last few decades, mainly attributed to accelerated surface warming [24,56,57]. On the contrary, annual area-averaged timeseries show no significant trend in area-averaged precipitation over 1979–2023. This is in contrast with previous studies investigating earlier periods showing a large reduction in *P*, especially within the western sub-basin, roughly occurring from the mid-1960s to mid-1990s and mainly attributed to an increasingly positive phase of North Atlantic Oscillation (NAO) [24,58]. Our results show that significant positive precipitation anomalies started to occur after the late 1990s following some strong negative phases of NAO over the more recent period, resulting in an overall very small and not statistically significant (at the 95% confidence interval) trend over 1979–2023. *E-P* total change averaged over the whole Mediterranean surface over 1979–2023 (~0.1 $\pm$ 0.03 m year^{-1} per 45 years) accounts for ~14% of the climatological mean. A recent analysis of river runoff data indicates no significant change in the total riverine freshwater input to the Mediterranean Sea since 1980 [59]. This is in contrast with large decreases in river freshwater input in the 1960s and 1970s, following the damming of the major Mediterranean rivers [60] (Ludwig et al., 2009). Therefore, if changes in total river runoff are neglected (i.e., based on Wang and Polcher [59]), a net evaporation increase of ~14% is obtained over the 1979–2023 period. This is still several times larger than global water cycle amplification estimates (e.g., ~3–4% over 1950–2010 [52]; ~3.6% over 1958–2016 [53]).

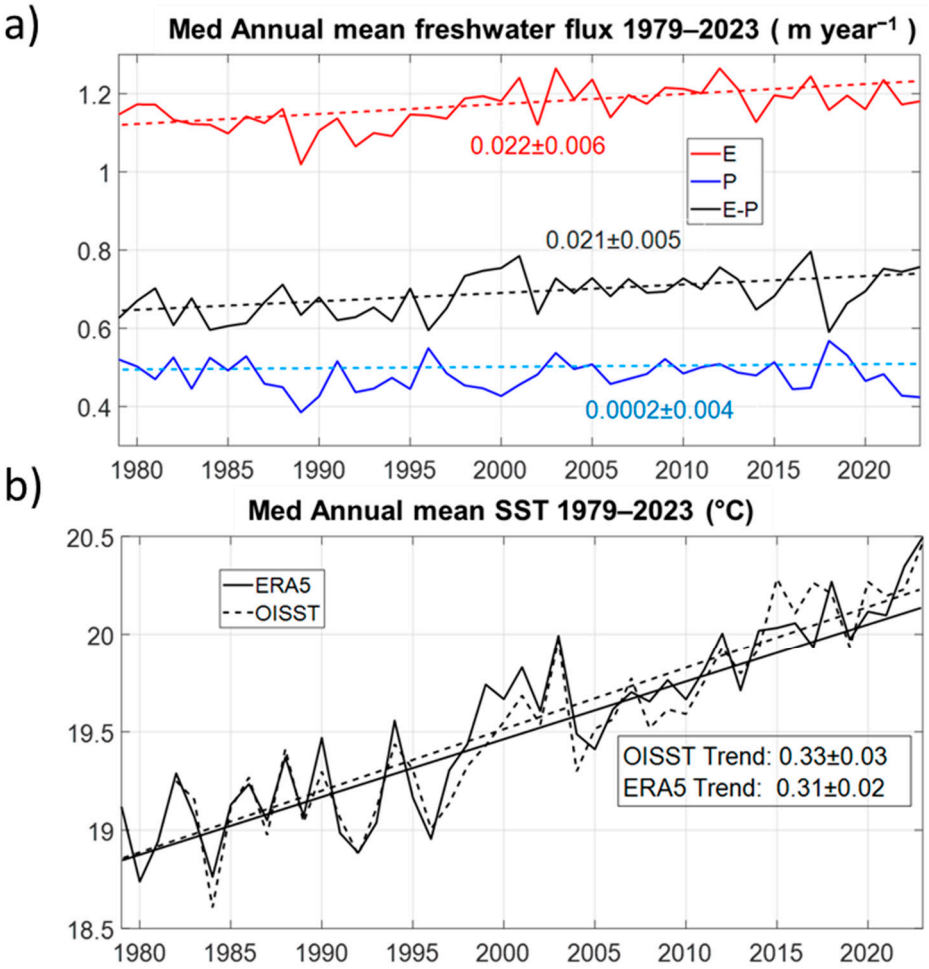

Figure 3. Annual timeseries of the total Mediterranean area-averaged timeseries over 1979–2023 of (**a**) *E* (red), *P* (blue), *E-P* (black) (in m year^{-1}), and (**b**) *SST* (black solid line) (°C) from ERA5. OISST annual mean timeseries (1982–2023) are also shown (dashed black line). Linear trends (±standard error) for freshwater fluxes (m year^{-1} per decade) and *SST* (°C per decade) are also depicted.

Results also show surface salinification across the basin (see Figure 2e), with statistically significant salinity increases exceeding 0.3 pss in most regions over 1979–2023. The largest salinity increases are obtained in the Adriatic, Ionian, and Tyrrhenian basins of ~1 pss. It is interesting to note that although both E-P and surface salinity trend patterns indicate very strong drying and salinification signals at the basin scale, they are not spatially consistent. In particular, in the Adriatic and North Aegean Seas, strong salinification trends are contrasted with no significant E-P trends, whereas in the southeastern part of the Levantine Basin, pronounced increases in E-P are contrasted with non-significant salinity trends. Although the water cycle is the major driver of surface salinity change in the global ocean, at regional/coastal scales, changes in ocean circulation and riverine inputs can largely control salinity variations. This is even more pronounced in a semi-enclosed basin as the Mediterranean, which is also characterised by intense coastal currents stirred by abrupt topography and a strong thermohaline (overturning) circulation that can efficiently propagate regional surface changes in hydrographic properties around the basin and into the deeper ocean. Moreover, well-documented long-term reduction in the Po River outflow and in the BSW inflow through the Dardanelles Straits can drive large increases in surface salinity in the Adriatic [61,62] and in the North Aegean [21,44], respectively. No significant trends in surface salinity are obtained in the Alboran Sea and in the northeast Atlantic adjacent to the Gibraltar Strait (see Figure 2e), suggesting the minimal contribution of the AW inflow to the broadscale salinification of the Mediterranean Sea.

3.1.2. Winter Surface Heat and Density Fluxes

Here, we investigate trends in air–sea flux components and associated surface (haline and thermal) density fluxes during winter (January–March) when intermediate/deep water formation occurs in the Mediterranean Sea [19,23]. We explore both spatial trend patterns (Figures 4 and 5) and area-averaged timeseries for the major four dense (intermediate and deep) water formation sites (Table 1), considering the long-term 1979–2023 period but also the most recent 20-year period (2004−2023) when significantly more substantial changes are obtained for surface heat and density fluxes. Ocean heat loss and associated surface density flux variability during winter are strongly controlled by turbulent heat fluxes (i.e., *LHF* and *SHF*) over the dense water formation sites in particular. Area-averaged timeseries of winter ocean net heat loss are very highly correlated in all four major dense water mass formation sites with both *LHF* ($r > 0.98$) and *SHF* ($r > 0.94$).

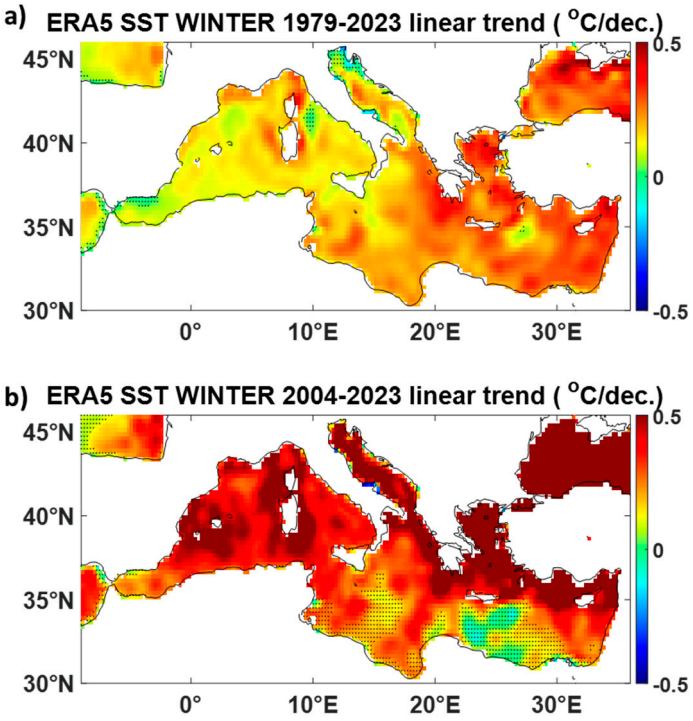

Figure 4. Spatial patterns of the linear trends in the winter (January–March) mean *SST* (°C per decade) for two periods: 1979–2023 (**a**) and 2004–2023 (**b**) (from ERA5). Regions where the linear trend is not statistically significant at the 95% confidence interval are stippled.

In contrast with annual trends, where the sea surface warming trend is similar in the two sub-basins, there is an eastward-increasing surface warming gradient during winter over 1979–2023 (Figure 4a). Timeseries of winter air–sea heat/freshwater fluxes and associated surface density fluxes show very strong interannual and decadal variability, reducing the statistical significance of trends over most of the Mediterranean surface (Figure 5). Differential warming seems to drive significant broadscale increases in *LHF* across the south part of EMED during winter (Figure 4a), driving increasing ocean heat loss over 1979–2023 (Figure 5a). On the contrary, no statistically significant long-term trends were obtained over the western basin and, importantly, over all four major dense water formation sites. However, our results show much stronger trends in all air–sea interaction parameters/fluxes over 2004–2023 (see Table 1). *SST* warming rates are almost two times larger with respect to long-term trends, with pronounced warming exceeding 0.5 °C per decade encountered in the Aegean and Adriatic Seas but now also in large parts of the western basin (Figure 4b). It is interesting to note that winter *SST* and *LHF* spatial

trend patterns (Figures 4b and 5d, respectively) are much less consistent with respect to annual trends (See Figure 2) over the NW Mediterranean in particular. During winter, turbulent heat flux anomalies are strongly regulated by larger wind intensity anomalies, especially over dense water formation sites. At the basin scale, much higher correlations are obtained here between area-averaged winter *LHF* anomalies and wind intensity anomalies (r~0.6) than *SST* anomalies (r~0.3). Results show spatially coherent and robust decreasing winter ocean heat loss driven by decreasing *LHF* and *SHF* trends in the NW Mediterranean, including the Gulf of Lions, over 2004–2023 (see Figure 5). On the contrary, over the same period, *LHF* and *SHF* increase drive a strong increase in winter ocean heat loss over the Aegean Sea. This is largely driven by a contrasting sea–air temperature difference (*SST*-T_{air}) trend between the two sub-basins, with WMED and the NW Mediterranean in particular showing much larger air warming than ocean surface warming, whilst the opposite occurs in large parts of EMED, especially in the Aegean Sea (Figure 5h). This pattern is consistent with the mechanism advanced for reduced winter heat loss in the NW Mediterranean found by Josey and Schroeder [18], i.e., air temperature has increased more rapidly than *SST* at multidecadal timescales, leading to weaker heat loss. Area-averaged timeseries of winter ocean heat loss and *SST*-T_{air} show very strong and highly statistically significant correlations (at the 99% confidence interval) over all major dense water formation sites (i.e., Gulf of Lions: r = 0.91; S. Adriatic: r = 0.92; Rhodes Gyre: r = 0.86; Aegean Sea: r = 0.92). It is interesting to note that although both turbulent flux trends are positive and negative in the Gulf of Lions and the Aegean Sea, respectively, *SHF* is the major contributor to reduced ocean heat loss in the Gulf of Lions, whereas *LHF* is the major contributor to increased ocean heat loss in the Aegean Sea.

Table 1. Linear trends in winter (January–March) mean *SST*, *SST*-T_{air}, *LHF*, *SHF*, D_T, D_S, and D_{TOT} in the major dense water formation sites of Gulf of Lions, S. Adriatic, Aegean, and Rhodes Gyre and for the periods 1979–2023 and 2004–2023, respectively.

	SST **(°C dec.$^{-1}$)**		***SST*-T_{air}** **(°C dec.$^{-1}$)**	
	1979–2023	**2004–2023**	**1979–2023**	**2004–2023**
Gulf of Lions	0.15 *	0.38 *	−0.05	−0.37 *
S. Adriatic	0.15 *	0.47 *	−0.09	−0.17
Aegean	0.28 *	0.61 *	−0.07	0.09
Rhodes Gyre	0.24 *	0.39 *	−0.03	0.11
	LHF **(W m^{-2} dec.$^{-1}$)**		***SHF*** **(W m^{-2} dec.$^{-1}$)**	
	1979–2023	**2004–2023**	**1979–2023**	**2004–2023**
Gulf of Lions	1.0	−6.4 *	−0.5	−6.5 *
S. Adriatic	0.7	2.7	−0.7	−1.4
Aegean	1.8	11.2 *	−0.9	2.5
Rhodes Gyre	2.3	5.1	−0.2	1.4
	D_T ($\times 10^{-7}$, kg m^{-2} s^{-1} dec.$^{-1}$)		**D_S ($\times 10^{-8}$, kg m^{-2} s^{-1} dec.$^{-1}$)**	
	1979–2023	**2004–2023**	**1979–2023**	**2004–2023**
Gulf of Lions	0.2	−6.1 *	2.9	−2.9
S. Adriatic	−0.2	−0.8	−1.2	22.2 *
Aegean	1.2	10.0 *	−1.1	12.4 *
Rhodes Gyre	1.4	4.6	3.8 *	3.7
	D_{TOT} ($\times 10^{-7}$, kg m^{-2} s^{-1} dec.$^{-1}$)			
	1979–2023	**2004–2023**		
Gulf of Lions	0.5	−6.4 *		
S. Adriatic	−0.3	3.0		
Aegean	1.1	11.3 *		
Rhodes Gyre	1.8	4.9		

* denotes trends that are statistically significant at the 95% confidence interval.

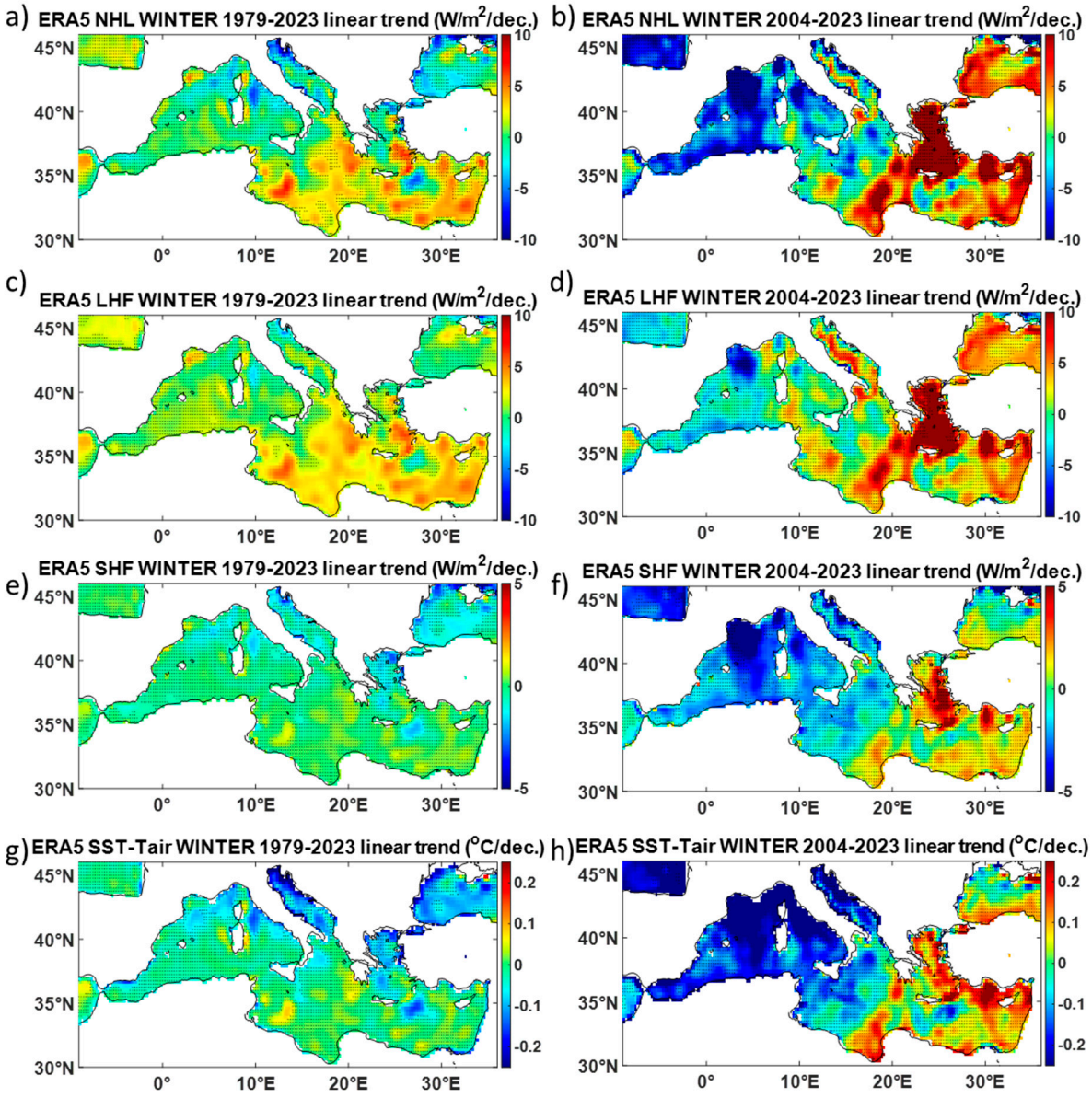

Figure 5. Spatial patterns of linear trends for periods 1979–2023 (left panels) and 2004–2023 (right panels in winter mean *NHL* (W m^{-2} per decade (**a**,**b**), *LHF* (W m^{-2} per decade) (**c**,**d**), *SHF* (W m^{-2} per decade) (**e**,**f**), and *SST-*T_{air} (°C per decade) (**g**,**h**). All data are taken from ERA5. *SHF*, *LHF*, and *NHL* are defined as positive (to the atmosphere). Regions where the linear trend is not statistically significant at the 95% confidence interval are stippled.

LHF is probably the major driver of dense water formation during wintertime in all Mediterranean deep water formation sites as surface waters become cooler and also saltier under strong cold and highly evaporative northerly winds. Large increases in winter *LHF* obtained here over EMED also drive large increases in the haline component of the surface density flux through increased evaporation. The resulting salinity increase may counterbalance the warming effect on density and, therefore, stratification. Although the thermal component (D_T) is the major contributor to total surface density flux (D_{TOT}) change, results show that the haline component (D_S) has a significant contribution, with especially large increases over most of the East Mediterranean Sea over 1979–2023 (Figure 6). In particular, over 2004–2023, D_S has increased strongly in the S. Adriatic and Aegean Seas whilst decreasing in the Gulf of Lions. Strong decreases in winter *SHF*/*LHF*/*E* over the Gulf of Lions contribute to a large reduction of the total surface density flux (D_{TOT}) over the last

20 years (see Figure 6). This is consistent with the observation of no significant deep water formation in WMED over the last decade [18,45].

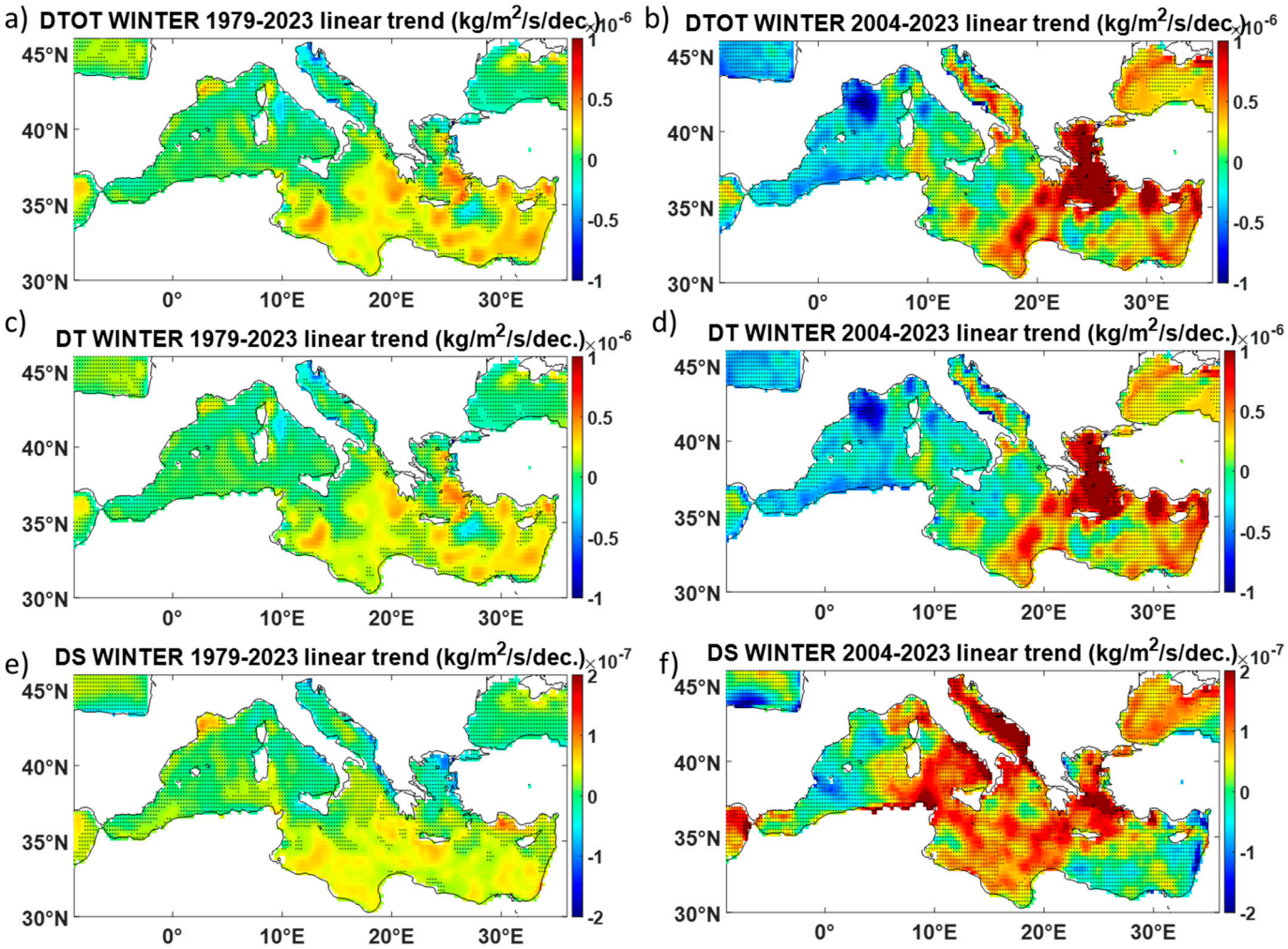

Figure 6. Spatial patterns of linear trends in winter (January–March) surface density fluxes, D_{TOT} (**a**,**b**), D_T (**c**,**d**), and D_S (**e**,**f**) (in kg m^{-2} s^{-1} per decade) over 1979–2023 (left panels) and 2004–2023 (right panels). Trends that are statistically not significant at the 90% confidence interval are stippled.

3.2. Hydrological Properties

3.2.1. Warming and Salinification Trends

Our analysis of the EN4 dataset shows a robust and spatially coherent structure of long-term strong salinification of the basin. Following the net evaporation increase, robust positive trends in salinity are evidenced throughout the basin, from surface to deep layers (Figure 7 and Table 2). Results show an increased salinification rate across the basin after the mid-2000s, except from the upper layer of WMED. Upper layer salinity variations show no significant changes until the late 1990s, but then salinity abruptly increases in both sub-basins (Figure 7a). Then, upper layer salinity shows an accelerating increase in EMED but no significant change in WMED over the last 2 decades.

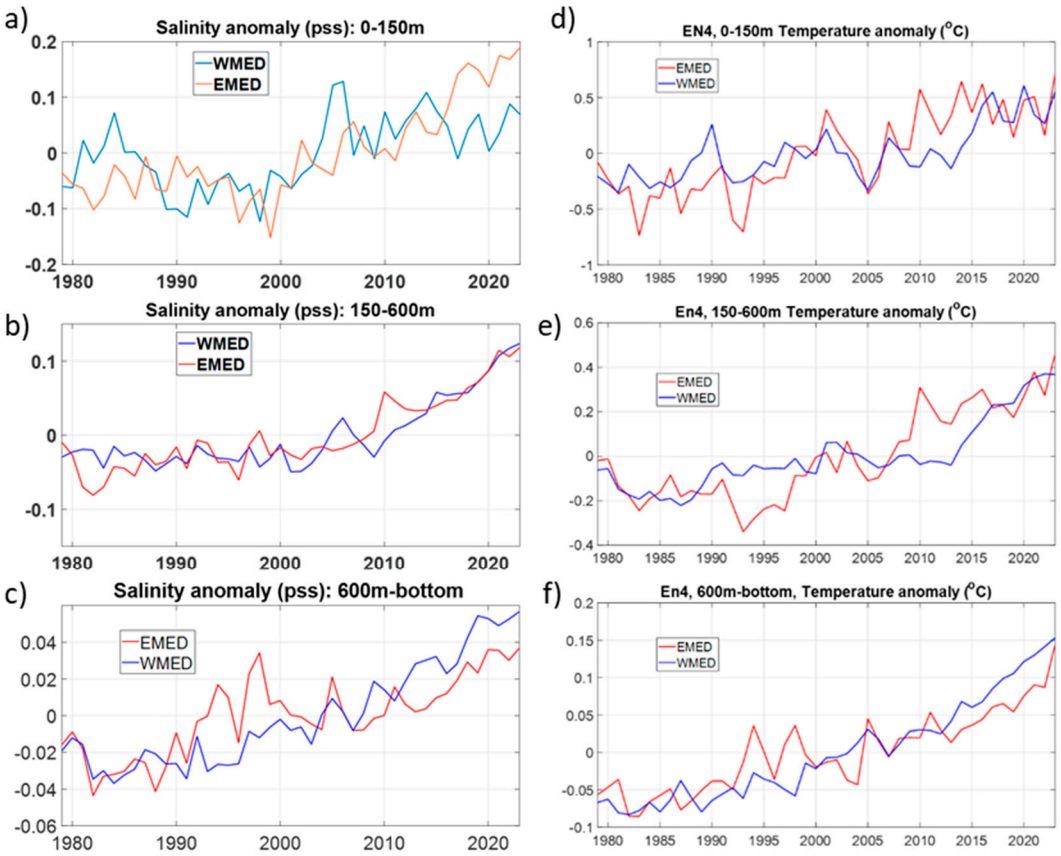

Figure 7. Annual mean timeseries of area-averaged anomalies of salinity (pss) (left panels) and temperature (°C) (right panels) for three depth layers—0 –150 m (**a**,**d**), 150–600 m (**b**,**e**), and 600 m bottom (**c**,**f**)—for East (red line) and West (blue line) Mediterranean sub-basins.

A quasi-continuous salinity increase is evidenced in the intermediate (150–600 m) layer of both sub-basins, again with an increased salinification rate after the mid-2000s (Figure 7b). This is the typical layer of the Levantine Intermediate Water (LIW) typically formed in the Rhodes Gyre, which then circulates around the Mediterranean, strongly controlling deep water formation in all major formation sites both in the eastern (Aegean, S. Adriatic) and western (Gulf of Lions) sub-basins. Therefore, continuous salinity increase in this layer is expected to enhance salt preconditioning for deep water formation. Salinity variations in the deep layer (>600 m) also show a general increasing trend but with pronounced interannual/decadal positive anomalies in both sub-basins (Figure 7c). These abrupt anomaly peaks reflect the excessive climate transient events (i.e., EMT peaking in the first half of the 1990s and WMT peaking in the second half of the 2000s), producing strong deep water formation over a few years (under anomalous winter cooling and enhanced salt preconditioning), thus efficiently propagating signals of saltier surface/intermediate waters to the deep ocean. Salinity variations in the deep layer may be considered a proxy for the strength of deep water formation and, therefore, of the Mediterranean overturning circulation. The salinification trends in intermediate and deep waters accelerating over the last two decades are indicative of intensifying zonal (intermediate layer) and deep overturning cells of both sub-basins over 1979–2023 despite the accelerating Mediterranean surface warming.

Table 2. Linear trends in annual mean volume-averaged salinity (pss per decade), temperature (°C per decade), and density (kg m^{-3} per decade) in WMED and EMED for the periods 1979–2023 and 2004–2023 and for the 0–150 m, 150–600 m, and 600 m bottom layers, respectively.

Salinity (pss dec.$^{-1}$)				
	WMED		**EMED**	
	1979–2023	**2004–2023**	**1979–2023**	**2004–2023**
0–150 m	0.028 *	−0.005	0.051 *	0.112 *
150–600 m	0.028 *	0.071 *	0.033 *	0.070 *
600 m bottom	0.019 *	0.032	0.013 *	0.021 *
Temperature (°C dec.$^{-1}$)				
	WMED		**EMED**	
	1979–2023	2004–2023	1979–2023	2004–2023
0–150 m	0.014 *	0.039 *	0.023 *	0.032 *
150–600 m	0.010 *	0.024 *	0.013 *	0.022 *
600 m bottom	0.049 *	0.077 *	0.036 *	0.057 *
Density (kgm^{-3} dec.$^{-1}$)				
	WMED		**EMED**	
	1979–2023	2004–2023	1979–2023	2004–2023
0–150 m	−0.013	−0.010	−0.016	0.008
150–600 m	−0.001	−0.004	−0.004	−0.003
600 m bottom	0.004 *	0.009 *	0.004 *	0.011 *

* denotes trends that are statistically significant at the 95% confidence interval.

Robust positive trends in temperature are also evidenced throughout the basin, from surface to deep layers, with an accelerated warming rate after the mid-2000s, closely following the salinification trend over the last 20 years. The abrupt shift in warming and salinification of intermediate/deep layers after the mid-2000s obtained here is consistent with various regional observational studies [9,21].

Density variations are dominated by stronger interannual and decadal signals. Increasing trends in upper and intermediate layer temperature and salinity almost counterbalance each other, resulting in not-significant long-term trends in area-averaged density in both sub-basins over 1979–2023 (Figure 8). Density variations in the deep layer show larger decadal variability (compared to T and S) with pronounced positive anomaly peaks mainly driven by the two major climate transient events (EMT, WMT). However, increasing salinity trends drive a small but significant long-term increase in the density of the deep layer of both sub-basins, indicating enhanced deep water formation. Quasi-continuous density increases obtained here in the deeper layer are in accordance with other observational regional studies for both EMED [21,40] and WMED [8,9] sub-basins.

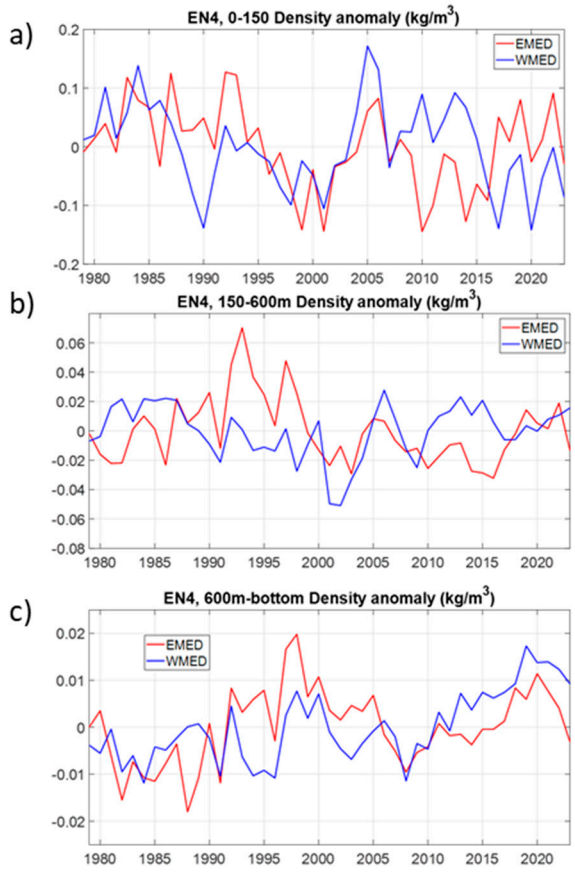

Figure 8. Annual mean timeseries of area-averaged anomalies of density (kg $m^{-3)}$ for three depth layers—0−150 m (**a**), 150−600 m (**b**), and 600 m–bottom (**c**)—for East (red line) and West (blue line) Mediterranean sub-basins.

3.2.2. Water Mass Transformation in Property Space

The volumetric distribution in salinity coordinates *V(S)* is discretised by intervals of ΔS = 0.01 pss (i.e., the volume of seawater (m^3) per 0.01 pss interval). Figure 9a shows the volumetric distributions in salinity space for nominal years 1979 and 2023 (based on the 3-D salinity linear trends over 1979–2023). Volumetric distribution for east and west sub-basins show two distinct peaks around 38.45 and 38.75 pss, representative of the average WMED and EMED deep water properties, respectively (Figure 9a). Volumetric change Δ*V(S)* since 1979 shows a large displacement of both volumetric distributions/peaks towards higher salinities as water masses become more saline throughout the basin. The cumulative water mass transformation rate in salinity space, i.e., integrating the transformation rate (volumetric change over 1979–2023) from low to high salinity, decreases (as volumes of relatively low salinity waters are reduced) until reaching a minimum (negative peak) around the basin-average salinity, and then it increases (as volumes of relatively high salinity are increased) to reach zero at the highest salinity (i.e., the integrated total volumetric change is zero as mass is conserved) (Figure 9b). The cumulative transformation rate is negative throughout the salinity space, indicating a displacement of volumes of water towards higher salinities across the basin (as waters become saltier), peaking at the volumetric peaks of the two sub-basins (Figure 9b). The maximum (negative) cumulative water mass transformation rate over 1979–2023 is higher in EMED, i.e., ~−0.8 Sv, than in WMED, i.e., ~−0.5 Sv. However, these results actually indicate a more drastic water mass transformation in the WMED, taking into account that the volume of EMED is approximately twice that of WMED. Results show that the water mass transformation rate is low at lower salinities representative of AW (from ~36.5 pss in the Alboran Sea to ~38.2 pss in the Levantine Basin). A recent

observational study based on ARGO data since the early 2000s shows either a small but statistically significant freshening trend or statistically not significant trends along the AW pathway in WMED [25]. Results suggest that the salinification of the Mediterranean Sea is largely driven by increasing net evaporation rather than changes in salt transports at the straits, in accordance with a previous study considering an earlier period [24].

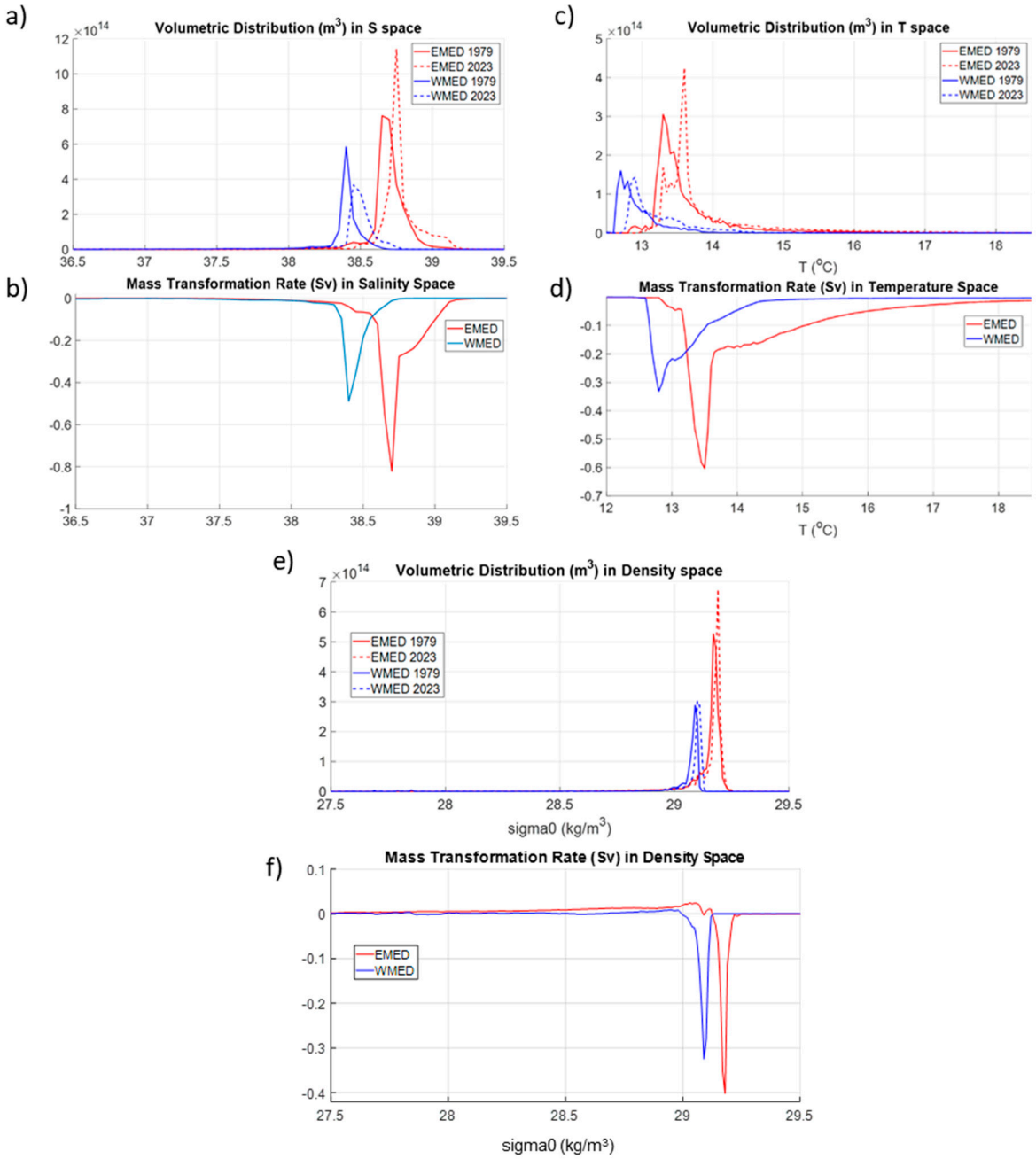

Figure 9. Volumetric distribution (m^3) in salinity (pss), temperature (°C), and density (kg m^{-3}) coordinates for nominal years 1979 (solid lines) and 2023 (dashed lines) (**a**,**c**,**e**) and cumulative water mass transformation rate (Sv = 10^6 m^3 s^{-1}) over 1979–2023 (**b**,**d**,**f**) for East (red) and West (blue) Mediterranean sub-basins.

Volumetric change in temperature space, $\Delta V(T)$ (discretised by intervals of $\Delta T = 0.05$ °C), since 1979 shows a large displacement of the two volumetric peaks (EMED and WMED) towards higher temperature (Figure 9c). As for salinity, the cumulative water mass transformation rate in T space (integrating from low to high temperature) is again negative

throughout the T space as volumes of water are displaced towards higher temperature, i.e., relatively cold water is transformed into warmer water across the basin (Figure 9d). However, maximum (negative) cumulative water mass transformation rates in T space, peaking at ~−0.6 Sv in EMED and ~−0.3 Sv in WMED, respectively, are significantly lower than those in S space, indicating that increasing salinity drives an overall increase in dense water formation over the whole basin despite strongly increasing surface warming.

As a consequence of opposing T and S trend contributions in density, the volumetric change in density space, $\Delta V(\rho)$ (discretised here by intervals of $\Delta\,\rho = 0.01$ kg m^{-3}), since 1979 (Figure 9e) shows a small but significant displacement of both volumetric peaks towards higher density, indicating that salinity change is still the major contributor to density change over most of the Mediterranean basin. Importantly, both volumetric peaks in density space, characteristic of deep waters, are presented at larger volumes in 2023, indicating overall increasing deep water formation in both sub-basins over 1979–2023. However, the cumulative water mass transformation rate in density space indicates a transformation into lighter waters at low densities (positive transformation) and a much stronger transformation into more dense waters at high densities (negative transformation) (Figure 9f). Maximum (negative) water mass transformation rates in density space in the two sub-basins are much closer than in T or S space, peaking at ~0.4 Sv in EMED and ~0.3 Sv in WMED, respectively. Taking into account the volumes of the two sub-basins, mass transformation in density space is again relatively more intense in WMED, similar to the mass transformation pattern in salinity space.

In order to look in more detail into the vertical structure of water mass transformation in density space, the transformation rates are calculated in three successive layers: upper (0–150 m), intermediate (150–600 m), and deep (600 m bottom) (Figure 10). The results clearly show opposing trends with the upper (0–150 m) layer and part of lower density intermediate layers, predominantly indicating a transformation into less dense waters contrasted with a transformation into much denser waters in the deeper layer. This contrasting pattern is much more pronounced in EMED, where excessive warming is the major driver of density change (despite the strong salinification trend), resulting in transformation into predominantly lighter waters in the upper layer. In the WMED upper layer, low-density waters characteristic of fresh AW inflow are also transformed into lighter waters. However, transformation rates (into predominantly lighter waters) in the major part of the upper layer of WMED are much less than in EMED. On the contrary, transformation into denser water within the intermediate layer is much more drastic in WMED as compared with EMED. In the latter, there is even a significant transformation into lighter waters at lower densities. The deep layer shows clear negative transformation peaks, with denser waters being produced in both sub-basins, closely following the transformation pattern in salinity space. Our analysis highlights the increasing density contrast between upper and deeper layers, pointing to a more stratified water column across the basin.

In the next step of our analysis, water mass transformation is explored in T/S coordinates, which is the natural space used to assess changes in water masses. The volumetric distribution of the whole Mediterranean basin is discretised here by intervals of $\Delta T = 0.05$ °C and $\Delta S = 0.01$ pss. Transformation rates over 1979–2023 within the three vertical layers are investigated once again, but now changes in winter (January–March) means are calculated to focus on the dense water formation period. For annual means, water mass transformation patterns are very similar to those of winter means, particularly in the intermediate and deep layers.

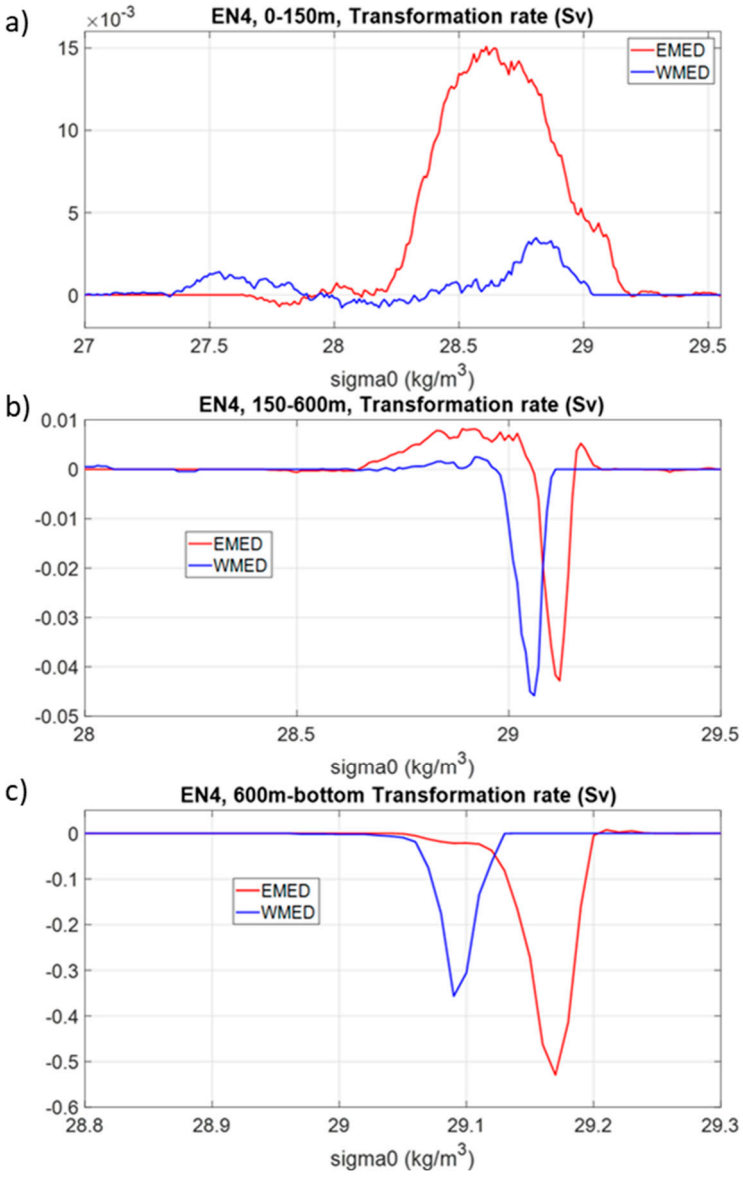

Figure 10. Cumulative water mass transformation rates (Sv = 10^6 m^3 s^{-1}) in density space over 1979–2023 in (**a**) the upper (0–150 m), (**b**) intermediate (150–600 m), and (**c**) deep (600 m bottom) layers for East (red) and West (blue) Mediterranean sub-basins.

The water mass transformation pattern (Figure 11) shows dipoles of negative/positive transformation rates that indicate large volume displacement in *T/S* space, i.e., volumes were displaced from relatively cold and fresh waters (decreased volume/negative mass transformation) to warmer and saltier waters (increased volume/positive mass transformation). Transformation into warmer and saltier waters is evidenced in the upper layer across the basin (Figure 11d). However, at low densities and near the surface, mainly occupied by Atlantic Water (AW), warming contributes to transformation rates, resulting in less dense waters. Salinity contribution becomes increasingly more important following the AW pathway from WMED into EMED, as well as in central/north parts of the basin, where the AW influence is much lower. In these regions, salinity contribution largely counterbalances the warming effect, resulting in transformations almost along isopycnals, indicating very small density changes. This pattern again suggests that the salinification of the basin is largely driven by changes in the regional water cycle rather than changes in AW freshwater transport through the Gibraltar Strait. In the upper layer of the eastern Levantine Basin partly occupied by LSW, characterised by the saltiest and warmest Mediterranean waters,

excessive warming is the larger contributor to water mass transformation, despite the large salinification trend, resulting in decreasing density over 1979–2023.

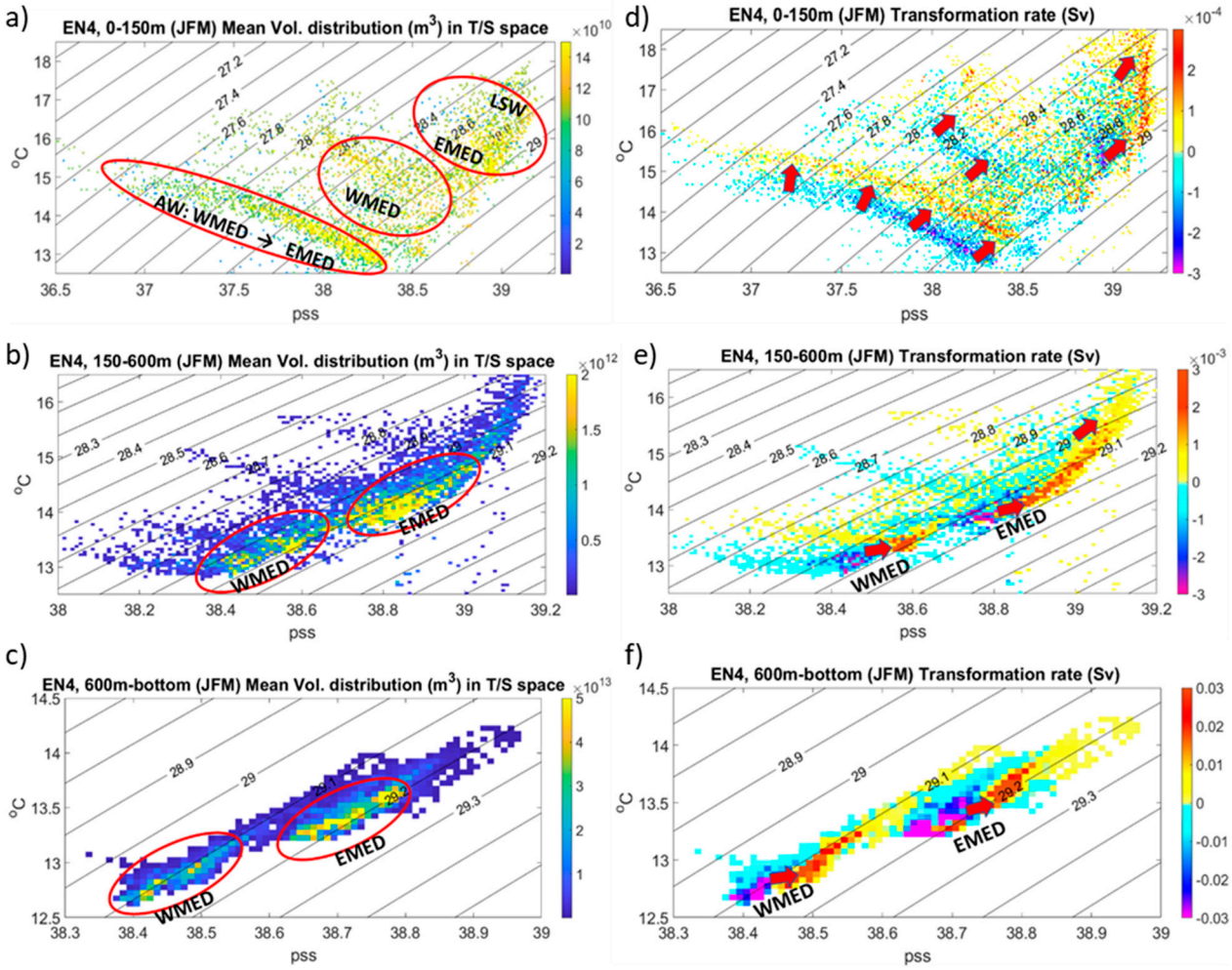

Figure 11. Mean volumetric distribution (m^3) (**a**,**c**,**e**) and water mass transformation rate (Sv) (**b**,**d**,**f**) in *T/S* space during winter (January–March) over 1979–2023 for three layers: upper (0–150 m), intermediate (150–600 m), and deep (600 m—bottom). Isopycnals (σ_0, kg m^{-3}) are also depicted (black solid lines). The bulk of large volumes of water representative of water masses in the two sub-basins (mainly LIW in the intermediate layer across the basin and EMDW and WMDW in the deep layer of EMED and WMED, respectively) are depicted with red circles. Volumes of fresh AW in the upper layer as it flows from WMED to EMED and LSW are also depicted. The mean direction of water mass transformation (water volume displacement in *T/S* space over 1979–2023) is depicted with red arrows to highlight cross-isopycnal transformations, i.e., indicating if more or less dense water is formed during this period.

Mass transformation into warmer and saltier waters is evidenced in the typical LIW layer (150–600 m) (Figure 11e). Transformation is mostly oriented across isopycnals, with salinification being the major contributor in most regions, resulting in the production of significantly denser waters in both sub-basins. An exception is the upper part of the intermediate layer of EMED, where excessive warming penetrates deeper. Transformation into warmer and saltier waters in the deep layer is also mostly oriented across isopycnals, in WMED in particular, with salinification being again the major contributor to density change, resulting in the production of significantly denser deep waters in both sub-basins (Figure 11f). Transformation in *T/S* space clearly highlights again the enhanced contrast between upper layer water masses (i.e., AW and LSW) predominantly becoming less dense

and intermediate (LIW) and particularly deep (EMDW, WMDW) water masses becoming denser over 1979–2023.

Mass transformations in *T/S* space are also calculated separately for the four major dense (intermediate and deep) water formation sites, i.e., the Aegean Sea, the Rhodes Gyre area, the S. Adriatic, and the Gulf of Lions (Figure 12). These regional transformations here are, of course, strongly controlled not only by local air–sea heat/freshwater fluxes but also by heat/freshwater transports across the open boundaries/straits. The transformation over 1979–2023 in all water formation sites follows the same general pattern of increasing transformation of waters towards higher temperatures and salinities, with predominantly larger salinity contributions transforming intermediate and particularly deep waters at higher densities. However, transformation patterns are more accentuated, with the whole bulk of various water masses drastically displaced in *T/S* space.

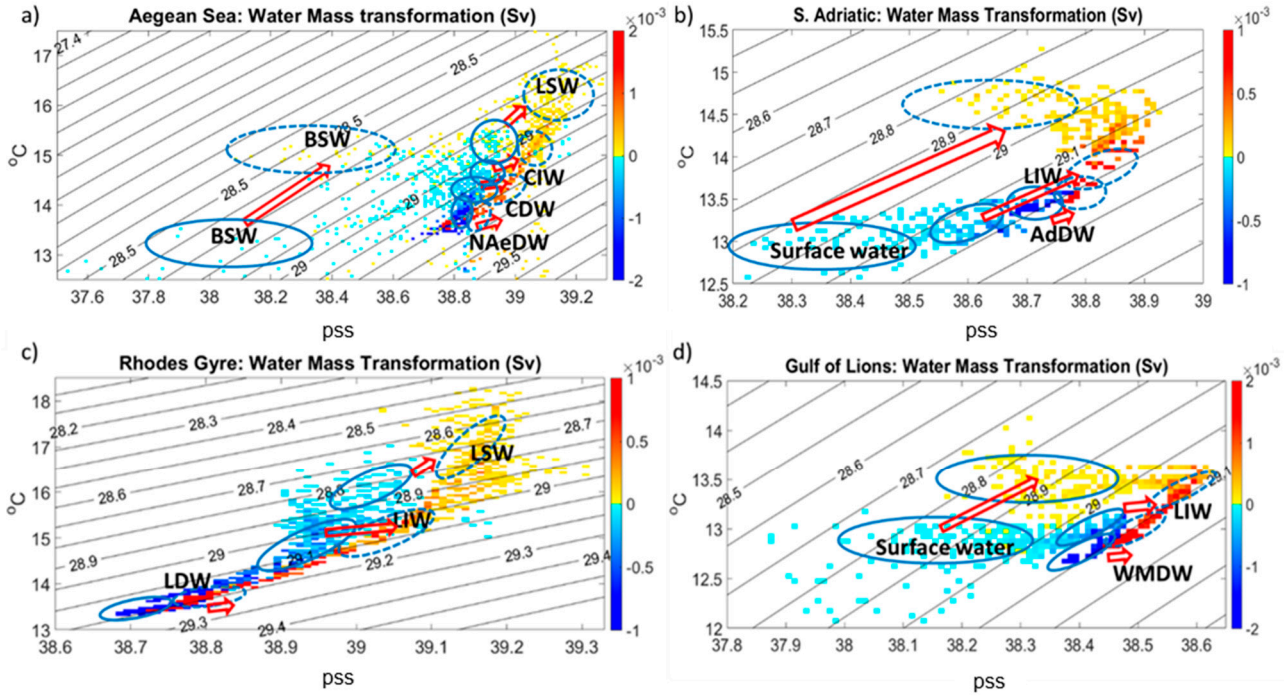

Figure 12. Water mass transformation rate (Sv) in *T/S* space during winter (January–March) over 1979–2023 spanning the whole water column and for four regions: Aegean Sea (**a**), South Adriatic Sea (**b**), Rhodes Gyre (**c**), and Gulf of Lions (**d**). Isopycnals (σ_0, kg m^{-3}) are also depicted (black solid lines). The bulk of large volumes of water representative of water masses in the two sub-basins, mainly LIW in the intermediate layer across all regions, and CIW/CDW/NAeDW (Aegean), ADW (South Adriatic), and WMDW (Gulf of Lions), respectively, are depicted with solid (1979) and dashed (2023) ellipses. The mean direction of water mass transformations (water volume displacement in *T/S* space over 1979–2023) is depicted with red arrows to highlight cross-isopycnal transformations, i.e., indicating if more or less dense water is formed during this period.

In the Aegean Sea (Figure 12a), transformations at lower densities in the upper layer primarily influenced by fresh/cold BSW intrusion show a large displacement towards higher temperatures (by ~1.5–2 °C) and salinities (by >0.2–0.4 pss), mostly along isopycnals. Decreasing BSW inflow was suggested to be a major salt preconditioning factor enhancing deep water formation in the North Aegean Sea during the EMT [21,63]. Transformation in the area of relatively salty/warm LSW in the upper layer again also shows large displacements towards higher salinity and temperature, but the warming (~2 °C) contribution to density change is larger, resulting in the transformation of mostly lighter waters. Areas of intermediate (CIW/LIW) waters and especially deep (NAeDW, CDW) waters show, in

contrast, large cross-isopycnal transformations driven by pronounced salinity increases over 1979–2023. Especially for NAeDW, average density increases by >0.1 kg m^{-3} with the large bulk of water denser than 29.2 kg m^{-3} formed during this period. This reflects both the EMT period (1987–1994), where exceptionally large volumes of deep water were formed in both the North Aegean and Cretan Seas under strong salt preconditioning, but also subsequent smaller EMT-type events [16,20] and a more recent pronounced salinification of intermediate waters under increasing atmospheric forcing and reduced BSW inflow [21,44].

In the Rhodes Gyre, as with the Aegean Sea, the surface layer mainly affected by LSW again shows large displacements towards higher salinity and temperature, but the excessive warming's (~2 °C) contribution to density change is larger, resulting in the transformation of mostly lower-density waters (Figure 12b). Transformation into saltier/warmer waters in the deep layer where Levantine Deep Water (LDW) is formed is considerably lower, and there is also much smaller cross-isopycnal displacement driven by salinity than in the Aegean Sea. The LIW layer is largely displaced in a warmer but much more saline *T/S* space with increased density. Almost isopycnal transformations into saltier/warmer waters are obtained in the Adriatic Sea over the whole water column, again with much smaller displacement in the deep layer where ADW is typically formed (Figure 12c). The larger Aegean Sea transformations and volume displacements within EMED over 1979–2023 reflect the large shift of the main source of deep water formation from the Adriatic to the Aegean Sea during the EMT.

In the Gulf of Lions, transformation in *T/S* space shows an excessive cross-isopycnal displacement of both intermediate (LIW) and deep (WMDW) layers driven by very strong increases in salinity. In particular, WMDW became saltier by >0.5 pss and denser by >0.5 kg m^{-3} over 1979–2023, with the large part of WMDW bulk being at σ_0 > 29.1 kg m^{-3}, largely reflecting the dramatic deep water formation increase in the region during WMT. On the contrary, the surface layer is displaced by lower warming and salinification trends, which seem to counterbalance each other, resulting in less pronounced and quasi-isopycnal transformations as compared with EMED surface waters.

4. Discussion and Conclusions

Our analysis suggests that the excessive basin-scale salinification was sufficient to sustain and even increase dense water formation in the Mediterranean Sea over 1979–2023 despite the accelerated warming over recent decades. Overall, denser intermediate and deep waters are produced over the 1979–2023 period in all major dense water mass formation sites, spreading across the basin. Long-term salinity increases in the Mediterranean Sea are consistent with increases in evaporation driven by surface warming obtained here in accordance with previous studies [24,55,56].

However, results suggest that a large part of long-term trends is mainly driven by extreme winter anomalous cooling events during the two major climatic transient events, i.e., EMT in the late 1980s/early 1990s and WMT in the mid-2000s. These transient events are mainly sustained by excessive turbulent (latent and sensible) heat fluxes during extreme cooling episodes over a few severe winters. Anomalous winter *SST* minus air temperature spatial patterns were also shown to significantly affect the intensity of the air–sea turbulent heat fluxes. Both sensible and latent heat fluxes show a long-term decreasing trend, resulting in a strong reduction of winter ocean heat loss in the Gulf of Lions over the last two decades. On the other hand, increased ocean heat loss driven primarily by *LHF* was observed in the Aegean Sea over the same period. These patterns are associated with a higher (lower) rate of air warming as compared to sea surface warming in the Gulf of Lions (Aegean Sea), consistent with the earlier findings of Josey and Schroeder (2023). Air–sea flux spatial trends over the last two decades are consistent with a possible eastward

shift in the locus of Mediterranean deep water formation towards the eastern basin, and the Aegean Sea in particular. The relatively small but significant salinity-driven density increases in the deep layer are consistent with winter surface density fluxes (as derived from the air–sea heat/freshwater fluxes), indicating a long-term increase in the contribution of the haline component to the surface density flux in EMED where LIW is produced. The strong salinification of LIW travelling across the basin can enhance salt preconditioning and sustain deep water formation of saltier/denser water in both sub-basins.

Our water mass transformation analysis in property space predominantly shows a transformation into lighter waters in the upper layer, primarily driven by warming, contrasted with a transformation into denser waters in the deeper layers, primarily driven by salinity change, suggesting an enhancement of stratification of the water column across the basin. This pattern is probably driven by processes acting at different timescales. Here, one needs to distinguish between the impacts of long-term increases in winter latent heat flux/evaporation driven by surface warming and the impacts of short-term (1–2 months) extreme winter cooling episodes involving excessive ocean heat loss and evaporation driven by anomalously strong latent heat flux. The two prominent climate transient events, i.e., EMT in the 1990s [31–33] and WMT in the mid-2000s [9,34] are initiated by anomalous (stronger) winter cooling episodes over one or two consecutive years under enhanced salt preconditioning, producing exceptionally large amounts of denser deep waters in deep water formations sites (i.e., in the Aegean Sea during EMT and in the Gulf of Lions during WMT). These very dense waters continued to outflow from the formation sites to the deeper EMED and WMED basins over the following few years, efficiently propagating warming and salinification surface signals towards deeper layers. Therefore, these major climate transient events were responsible for a pronounced warming and salinification of the deeper parts of EMED and WMED sub-basins at decadal scales. On the other hand, continuous long-term surface warming dominates density change in the upper layer, especially in EMED. Long after the EMT and WMT events, salinity-driven increased density signals seem to still propagate into the deep layer of both sub-basins until the end of 2010s, despite decreasing densities in large portions of the upper layer across the basin following the acceleration of surface warming. In EMED, smaller but still efficient EMT-type dense water formation episodes are evidenced [20,21] that are responsible for the replenishment of intermediate/deep waters with saltier/denser waters. In WMED, where no significant deep water formation has been reported over the last decade [18,45], salinity-driven signals may also be propagating from a saltier LIW layer into the deep layer after the WMT via the salt fingering process evidenced in the western basin [8].

However, there are still very large uncertainties and unanswered questions regarding the current status of the overturning/dense water formation and the drivers of their variability, mainly due to the disparity of subsurface hydrographic observations, especially within the Eastern Mediterranean, as well as uncertainties associated with atmospheric reanalyses. There are also large uncertainties due to the various complex physical processes acting at different timescales involved in the air–sea interaction, i.e., convective mixing (short term: days–weeks) and interior mixing (long term: years–decades), which makes observations and numerical modelling of dense water formation processes particularly difficult.

The increasing density contrast between upper and deep layers across the basin may have a strong negative impact on future deep water formation as stronger winter cooling episodes will be needed to destroy the enhanced stratification. Especially increasing stratification combined with long-term decreasing net heat loss over the Gulf of Lions, primarily driven by a much faster warming of the air compared to *SST* warming, may have severe implications for the future status of WMED overturning cells. This feature is also evidenced in regional climate models projecting a strong reduction of WMDW formation during this

century [46,48]. Although regional climate model projections show large discrepancies between models [46], most simulations also point to a (smaller) reduction of deep water formation in the East Med (S. Adriatic/Aegean) in the near future.

The latest IPCC report (AR6) states with high confidence that both warming and drought severity/intensity will strongly increase in the Mediterranean region during this century [64]. However, there are large uncertainties regarding the projected future status of the Mediterranean overturning during this century, as highlighted by the large discrepancies between different regional climate models (MED-CORDEX, [46]. Regional climate model projections indicate a substantial reduction in deep water formation throughout the basin as warming will become the main driver of stratification, with salinity increase not being sufficient anymore to counterbalance the stronger warming effect on density [46]. However, regional climate model responses regarding the WMED overturning cell seem to be particularly sensitive to predicted changes in the Atlantic inflow by each model [46]. However, the highest variance between climate model projections remains in the North/Central Aegean Sea, the region directly affected by the Black Sea low-salinity outflow strongly regulating local dense-water formation there, a fact possibly attributed to differences in simulating the exchange and its impact on local overturning [21,44,63]. Therefore, it remains uncertain whether the gradually stronger salt preconditioning in EMED will be sustained in the future as potential freshening of Black Sea inflow could at least partially counterbalance strong salinity increases in the Levantine Basin under drier conditions. The projected evolution of the freshwater budget of the Black Sea (controlled by rainfall over its large catchment area in Central–Eastern Europe) is critical to the fate of stratification in the Aegean Sea [21,44].

The resolution of the current generation of coupled ocean/atmosphere climate models is too low to properly capture open sea/shelf-dense water formation processes and reproduce abrupt climate transient events under extreme atmospheric forcing episodes during winter. More recent higher-resolution regional climate model simulations show a more drastic decrease in deep water formation in both sub-basins and even a collapse of the Western Med deep overturning cell in the next few decades [47,48]. On the other hand, re-analyses and observational datasets indicate much larger net evaporation increases over the Mediterranean compared to historical climate simulations [24,57]. This suggests that net evaporation/salinity increases could be considerably larger than that projected by the current generation of regional climate models, affecting their predictability of the future overturning circulation state. In general, there are also large uncertainties in both observing and predicting the water cycle and, subsequently, salinity changes at global and regional scales [65]. Especially the Mediterranean region is at the crossroads of large-scale natural climate variability modes/atmospheric teleconnections (e.g., North Atlantic Oscillation (NAO), East Atlantic Pattern (EAP), Atlantic Multidecadal Oscillation, African monsoon/Sahel rainfall, the South Asian Summer Monsoon (SASM), and the monsoon–desert teleconnection), strongly regulating the regional heat fluxes [66] and the water cycle and affecting their predictability by climate models. Assessing future changes in Mediterranean dense water formation is therefore important to better assess both long-term and abrupt changes in the large-scale atmospheric circulation and air–sea heat and freshwater fluxes over the Mediterranean Sea, as well as freshwater/heat transports at its straits.

Author Contributions: Conceptualization, N.S. and R.M.; methodology, N.S. and R.M.; validation, N.S., R.M., M.B. and S.A.J.; formal analysis, N.S and M.B.; investigation, N.S.; resources, N.S. and M.B.; data curation, N.S. and M.B.; writing—original draft preparation, N.S.; writing—review and editing, N.S., R.M., M.B. and S.A.J.; visualization, N.S.; supervision, N.S.; project administration, N.S. All authors have read and agreed to the published version of the manuscript.

Funding: This research received no external funding.

Institutional Review Board Statement: Not applicable.

Informed Consent Statement: Not applicable.

Data Availability Statement: The ECMWF ERA5 re-analysis monthly data (https://doi.org/10.24381/cds.f17050d7) are provided by the E.U. Copernicus Marine Service (https://cds.climate.copernicus.eu/datasets/reanalysis-era5-single-levels-monthly-means?tab=overview (accessed on 25 March 2024)). The UK Met Office Hadley Centre Enhanced Ocean Data Assimilation and Climate prediction (ENACT), archive version 4 (EN4, subversion En4.2.2(g10.analyses) is provided by Met Office UK (http://www.metoffice.gov.uk/hadobs/en4 (accessed on 25 March 2024)). NOAA Optimal Interpolated Sea Surface Temperature (OISST, version 2) monthly dataset is provided by PSL NOAA (https://psl.noaa.gov/data/gridded/data.noaa.oisst.v2.highres.html (accessed on 25 March 2024)).

Conflicts of Interest: The authors declare no conflicts of interest.

References

1. Giorgi, F. Climate change hot-spots. *Geophys. Res. Lett.* **2006**, *33*, L08707. [CrossRef]
2. Schroeder, K.; Chiggiato, J.; Josey, S.A.; Borghini, M.; Aracri, S.; Sparnocchia, S. Rapid response to climate change in a marginal sea. *Sci. Rep.* **2017**, *7*, 4065. [CrossRef] [PubMed]
3. Cheng, L.J.; Abraham, J.; Trenberth, K.E.; Boyer, T.; Michael, E.; Mann, M.E.; Zhu, J.; Wang, F.; Yu, F.; Locarnini, R.; et al. New record ocean temperatures and related climate indicators in 2023. *Adv. Atmos. Sci.* **2024**, *41*, 1068–1082. [CrossRef]
4. Mohamed, B.; Skliris, N. Steric and atmospheric contributions to interannual sea level variability in the eastern mediterranean sea over 1993–2019. *Oceanologia* **2022**, *64*, 50–62. [CrossRef]
5. Calafat, F.M.; Frederikse, T.; Horsburgh, K. The sources of sea-level changes in the Mediterranean Sea since 1960. *J. Geophys. Res. Oceans* **2022**, *127*, e2022JC019061. [CrossRef]
6. Kelley, C.; Ting, M.; Seager, R.; Kushnir, Y. The relative contributions of radiative forcing and internal climate variability to the late 20th Century winter drying of the Mediterranean region. *Clim. Dyn.* **2012**, *38*, 2001–2015. [CrossRef]
7. Cook, B.I.; Anchukaitis, K.J.; Touchan, R.; Meko, D.M.; Cook, E.R. Spatiotemporal drought variability in the Mediterranean over the last 900 years. *J. Geophys. Res. Atmos.* **2016**, *121*, 2060–2074. [CrossRef]
8. Borghini, M.; Bryden, H.; Schroeder, K.; Sparnocchia, S.; Vetrano, A. The Mediterranean is becoming saltier. *Ocean Sci.* **2014**, *10*, 693–700. [CrossRef]
9. Schroeder, K.; Chiggiato, J.; Bryden, H.L.; Ismail, S.B. Abrupt climate shift in the Western Mediterranean Sea. *Sci. Rep.* **2016**, *6*, 23009. [CrossRef]
10. Iona, A.; Theodorou, A.; Sofianos, S.; Watelet, S.; Troupin, C.; Beckers, J.M. Mediterranean Sea climatic indices: Monitoring long-term variability and climate changes. *Earth Syst. Sci. Data* **2018**, *10*, 1829–1842. [CrossRef]
11. Menna, M.; Gacic, M.; Martellucci, R.; Notarstefano, G.; Fedele, G.; Mauri, E.; Gerin, R.; Poulain, P.-M. Climatic, Decadal, and Interannual Variability in the Upper Layer of the Mediterranean Sea Using Remotely Sensed and In-Situ Data. *Remote Sens.* **2022**, *14*, 1322. [CrossRef]
12. Reale, M.; Cossarini, G.; Lazzari, P.; Lovato, T.; Bolzon, G.; Masina, S.; Solidoro, C.; Salon, S. Acidification, deoxygenation, and nutrient and biomass declines in a warming Mediterranean Sea. *Biogeosciences* **2022**, *19*, 4035–4065. [CrossRef]
13. Sisma-Ventura, G.; Ruth Yam, R.; Shemesh, A. Vermetid-derived sea surface temperature and δ13C DIC reconstructions for the eastern Mediterranean over the last millennium. *Geophys. Res. Lett.* **2014**, *41*, 5158–5166. [CrossRef]
14. Darmaraki, S.; Somot, S.; Sevault, F.; Nabat, P. Past variability of Mediterranean Sea marine heatwaves. *Geophys. Res. Lett.* **2019**, *46*, 9813–9823. [CrossRef]
15. Simon, A.; Pires, C.; Frölicher, T.L.; Russo, A. Long-term warming and interannual variability contributions' to marine heatwaves in the Mediterranean. *Weather. Clim. Extrem.* **2023**, *42*, 100619. [CrossRef]
16. Velaoras, D.; Krokos, G.; Nittis, K.; Theocharis, A. Dense intermediate water outflow from the Cretan Sea: A salinity driven, recurrent phenomenon, connected to thermohaline circulation changes. *J. Geophys. Res. Oceans* **2014**, *119*, 4797–4820. [CrossRef]
17. Taillandier, V.; D'Ortenzio, F.; Prieur, L.; Conan, P.; Coppola, L.; Cornec, M.; Dumas, F.; de Madron, X.D.; Fach, B.; Fourrier, M.; et al. Sources of the Levantine intermediate water in winter 2019. *J. Geophys. Res. Oceans* **2022**, *127*, e2021JC017506. [CrossRef]
18. Josey, S.A.; Schroeder, K. Declining winter heat loss threatens continuing ocean convection at a Mediterranean dense water formation site. *Environ. Res. Lett.* **2023**, *18*, 02400. [CrossRef]
19. Pinardi, N.; Estournel, C.; Cessi, P.; Escudier, R.; Lyubartsev, V. Dense and deep water formation processes and Mediterranean overturning circulation. In *Oceanography of the Mediterranean Sea*; Elsevier: Amsterdam, The Netherlands, 2023; pp. 209–261.

20. Velaoras, D.; Papadopoulos, V.P.; Kontoyiannis, H.; Papageorgiou, D.K.; Pavlidou, A. The response of the Aegean Sea (eastern Mediterranean) to the extreme 2016–2017 winter. *Geophys. Res. Lett.* **2017**, *44*, 9416–9423. [CrossRef]
21. Potiris, M.; Mamoutos, I.G.; Tragou, E.; Zervakis, V.; Kassis, D.; Ballas, D. Dense Water Formation Variability in the Aegean Sea from 1947 to 2023. *Ocean* **2024**, *5*, 611–636. [CrossRef]
22. Durrieu de Madron, X.; Houpert, L.; Puig, P.; Sanchez-Vidal, A.; Testor, P.; Bosse, A.; Estournel, C.; Somot, S.; Bourrin, F.; Bouin, M.N.; et al. Interaction of dense shelf water cascading and open-sea convection in the northwestern Mediterranean during winter 2012. *Geophys. Res. Lett.* **2013**, *40*, 1379–1385. [CrossRef]
23. Pinardi, N.; Zavatarelli, M.; Adani, M.; Coppini, G.; Fratianni, C.; Oddo, P.; Simoncelli, S.; Tonani, M.; Lyubartsev, V.; Dobricic, S.; et al. Mediterranean Sea large-scale low-frequency ocean variability and water mass formation rates from 1987 to 2007: A retrospective analysis. *Prog. Oceanogr.* **2015**, *132*, 318–332. [CrossRef]
24. Skliris, N.; Zika, J.D.; Herold, L.A.; Josey, S.; Marsh, R. Mediterranean Sea water budget long-term trend inferred from salinity observations. *Clim. Dyn.* **2018**, *51*, 2857–2876. [CrossRef]
25. Fedele, G.; Mauri, E.; Notarstefano, G.; Poulain, P.M. Characterization of the Atlantic Water and Levantine Intermediate Water in the Mediterranean Sea using 20 years of Argo data. *Ocean Sci.* **2022**, *18*, 129–142. [CrossRef]
26. Skliris, N.; Marsh, R.; Josey, S.A.; Good, S.A.; Liu, C.; Allan, R.P. Salinity changes in the World Ocean since 1950 in relation to changing surface freshwater fluxes. *Clim. Dyn.* **2014**, *43*, 709–736. [CrossRef]
27. Rahmstorf, S. Influence of Mediterranean outflow on Climate. *EOS* **1998**, *79*, 281–282. [CrossRef]
28. Artale, V.; Calmanti, S.; Malanotte-Rizzoli, P.; Pisacane, G.; Rupolo, V.; Tsimplis, M. The Atlantic and Mediterranean Sea as connected systems. Mediterranean Climate Variability. In *Developments in Earth and Environmental Sciences*; Lionello, P., Malanotte-Rizzoli, P., Boscolo, R., Eds.; Elsevier: Amsterdam, The Netherlands, 2006; Volume 4, pp. 283–323.
29. Aldana-Campino, A.; Döös, K. Mediterranean overflow water in the North Atlantic and its multidecadal variability. *Tellus A Dyn. Meteorol. Oceanogr.* **2020**, *72*, 1565027. [CrossRef]
30. Li, G.; Cheng, L.; Zhu, J.; Kevin, E.; Trenberth, K.E.; Michael, E.; Mann, M.E.; Abraham, J.P. Increasing ocean stratification over the past half-century. *Nat. Clim. Chang.* **2020**, *10*, 1116–1123. [CrossRef]
31. Roether, W.; Manca, B.B.; Klein, B.; Bregant, D.; Georgopoulos, D.; Beitzel, V.; Kovacevic, V.; Luchetta, A. Recent changes in the eastern Mediterranean deep waters. *Science* **1996**, *271*, 333–335. [CrossRef]
32. Klein, B.; Roether, W.; Manca, B.B.; Bregant, D.; Beitzel, V.; Kovacevic, V.; Luchetta, A. The large deep water transient in the Eastern Mediterranean. *Deep. Sea Res. Part I* **1999**, *46*, 371–414. [CrossRef]
33. Lascaratos, A.; Roether, W.; Nittis, K.; Klein, B. Recent changes in deep water formation and spreading in the eastern Mediterranean Sea: A review. *Prog. Oceanogr.* **1999**, *44*, 5–36. [CrossRef]
34. Zunino, P.; Schroeder, K.; Vargas-Yáñez, M.; Gasparini, G.P.; Coppola, L.; García-Martínez, M.C.; Moya-Ruiz, F. Effects of the Western Mediterranean Transition on the resident water masses: Pure warming, pure freshening and pure heaving. *J. Mar. Syst.* **2012**, *96–97*, 15–23. [CrossRef]
35. Roether, W.; Klein, B.; Manca, B.B.; Theocharis, A.; Kioroglou, S. Transient Eastern Mediterranean deep waters in response to the massive dense-water output of the Aegean Sea in the 1990s. *Prog. Oceanogr.* **2007**, *74*, 540–571. [CrossRef]
36. Schroeder, K.; Gasparini, G.P.; Tangherlini, M.; Astraldi, M. Deep and intermediate water in the western Mediterranean under the influence of the Eastern Mediterranean Transient. *Geophys. Res. Lett.* **2006**, *33*. [CrossRef]
37. Schroeder, K.; Ribotti, A.; Borghini, M.; Sorgente, R.; Perilli, A.; Gasparini, G.P. An extensive western Mediterranean deep water renewal between 2004 and 2006. *Geophys. Res. Lett.* **2008**, *35*. [CrossRef]
38. Millot, C.; Candela, J.; Fuda, J.-L.; Tber, Y. Large warming and salinification of the Mediterranean outflow due to changes in its composition. *Deep. Sea Res. Part I* **2006**, *53*, 656–666. [CrossRef]
39. Potter, R.A.; Lozier, M.S. On the warming and salinification of the Mediterranean outflow waters in the North Atlantic. *Geophys. Res. Lett.* **2004**, *31*, L01202. [CrossRef]
40. Martellucci, R.; Menna, M.; Mauri, E.; Pirro, A.; Gerin, R.; de Mendoza, F.P.; Garić, R.; Batistić, M.; di Biagio, V.; Giordano, P.; et al. Recent changes of the dissolved oxygen distribution in the deep convection cell of the southern Adriatic Sea. *J. Mar. Syst.* **2024**, *245*, 10398. [CrossRef]
41. Potiris, M.; Mamoutos, I.G.; Tragou, E.; Zervakis, V.; Kassis, D.; Ballas, D. Dense Water Formation in the North–Central Aegean Sea during Winter 2021–2022. *J. Mar. Sci. Eng.* **2024**, *12*, 221. [CrossRef]
42. Hayes, D.; Zodiatis, G.; Georgiou, G.; Mauri, E.; Poulain, P.; Gerin, R.; Notarstefano, G.; Testor, P. Changes in Levantine Intermediate Water properties observed in the eastern Levantine: 1995–2012. *Rapp. Comm. Int. Medit.* **2013**, *40*, 212.
43. Mihanović, H.; Vilibić, I.; Šepić, J.; Matić, F.; Ljubešić, Z.; Mauri, E.; Gerin, R.; Notarstefano, G.; Poulain, P.-M. Observation, preconditioning and recurrence of exceptionally high salinities in the Adriatic Sea. *Front. Mar. Sci.* **2021**, *8*, 672210. [CrossRef]
44. Mamoutos, I.G.; Potiris, E.; Androulidakis, Y.; Tragou, E.; Zervakis, V. Evidence for reduced Black Seawater outflow to the North Aegean. *Earth Space Sci.* **2024**, *11*, e2024EA003674. [CrossRef]

45. Margirier, F.; Testor, P.; Heslop, E.; Mallil, K.; Bosse, A.; Houpert, L.; Mortier, L.; Bouin, M.-N.; Coppola, L.; D'Ortenzio, F.; et al. Abrupt warming and salinification of intermediate waters interplays with decline of deep convection in the Northwestern Mediterranean Sea. *Sci. Rep.* **2020**, *10*, 20923. [CrossRef]
46. Soto-Navarro, J.; Jordá, G.; Amores, A.; Cabos, W.; Somot, S.; Sevault, F.; Macías, D.; Djurdjevic, V.; Sannino, G.; Li, L.; et al. Evolution of Mediterranean Sea water properties under climate change scenarios in the Med-CORDEX ensemble. *Clim. Dyn.* **2020**, *54*, 2135–2165. [CrossRef]
47. Parras-Berrocal, I.M.; Vázquez, R.; Cabos, W.; Sein, D.V.; Álvarez, O.; Bruno, M.; Izquierdo, A. Dense water formation in the eastern Mediterranean under a global warming scenario. *Ocean Sci.* **2023**, *19*, 941–952. [CrossRef]
48. Parras-Berrocal, I.M.; Vázquez, R.; Cabos, W.; Sein, D.V.; Álvarez, O.; Bruno, M.; Izquierdo, A. Surface and intermediate water changes triggering the future collapse of deep water formation in the North Western Mediterranean. *Geophys. Res. Lett.* **2022**, *49*, e2021GL095404. [CrossRef]
49. Hersbach, H.; Bell, B.; Berrisford, P.; Hirahara, S.; Horányi, A.; Muñoz-Sabater, J.; Nicolas, J.; Peubey, C.; Radu, R.; Schepers, D.; et al. The ERA5 global reanalysis. *Q. J. R. Meteorol. Soc.* **2020**, *146*, 1999–2049. [CrossRef]
50. Zika, J.D.; Skliris, N.; Nurser, G.; Josey, S.A.; Mudryk, L.; Laliberte, F.; Marsh, R. Maintenance and broadening of the ocean's salinity distribution by the water cycle. *J. Clim.* **2015**, *28*, 9550–9560. [CrossRef]
51. Walin, G. On the relation between sea-surface heat flow and thermal circulation in the ocean. *Tellus* **1982**, *34*, 187–195. [CrossRef]
52. Skliris, N.; Zika, J.D.; Nurser, G.; Josey, S.A.; Marsh, R. Global water cycle amplifying at less than the Clausius-Clapeyron rate. *Sci. Rep.* **2016**, *6*, 38752. [CrossRef]
53. Zika, J.D.; Skliris, N.; Marsh, R.; Blaker, A.T.; Nurser, G.; Josey, S.A. Improved estimates of water cycle change from ocean salinity. *Environ. Res. Lett.* **2018**, *13*, 074036. [CrossRef]
54. Hieronymus, M.; Nilsson, J.; Nycander, J. Water Mass Transformation in Salinity–Temperature Space. *J. Phys. Oceanogr.* **2014**, *44*, 2547–2568. [CrossRef]
55. Romanou, A.; Tselioudis, G.; Zerefos, C.S.; Clayson, C.; Curry, J.A.; Andersson, A. Evaporation–precipitation variability over the Mediterranean and the Black Seas from satellite and reanalysis estimates. *J. Clim.* **2010**, *23*, 5268–5287. [CrossRef]
56. Skliris, N.; Sofianos, S.; Gkanasos, A.; Mantziafou, A.; Vervatis, V.; Axaopoulos, P.; Lascaratos, A. Decadal scale variability of sea surface temperature in the Mediterranean Sea in relation to atmospheric variability. *Ocean Dyn.* **2012**, *62*, 13–30. [CrossRef]
57. Mariotti, A.; Pan, Y.; Zeng, N.; Alessandri, A. Long-term climate change in the Mediterranean region in the midst of decadal variability. *Clim. Dyn.* **2015**, *44*, 1437–1456. [CrossRef]
58. Krahmann, G.; Schott, F. Long-term increases in Western Mediterranean salinities and temperatures: Anthropogenic and climatic sources. *Geophys. Res. Lett.* **1998**, *25*, 4209–4212. [CrossRef]
59. Wang, F.; Polcher, J. Assessing the freshwater flux from the continents to the Mediterranean Sea. *Sci. Rep.* **2019**, *9*, 8024. [CrossRef]
60. Ludwig, L.; Dumont, E.; Meybeck, M.; Heussner, S. River discharges of water and nutrients to the Mediterranean and Black Sea: Major drivers for ecosystem changes during past and future decades? *Prog. Oceanogr.* **2009**, *80*, 199–217. [CrossRef]
61. Kokkini, Z.; Mauri, E.; Gerin, R.; Poulain, P.M.; Simoncelli, S.; Notarstefano, G. On the salinity structure in the South Adriatic as derived from float and glider observations in 2013–2016. *Deep. Sea Res. Part II* **2020**, *171*, 104625. [CrossRef]
62. Montanari, A.; Nguyen, H.; Rubinetti, S.; Ceola, S.; Galelli, S.; Rubino, A.; Zanchettini, D. Why the 2022 Po River drought is the worst in the past two centuries. *Sci. Adv.* **2022**, *9*, eadg8304. [CrossRef]
63. Zervakis, V.; Georgopoulos, D.; Drakopoulos, P.G. The role of the North Aegean in triggering the recent eastern Mediterranean climatic changes. *J. Geophys. Res. Oceans* **2000**, *105*, 26103–26116. [CrossRef]
64. Lee, J.-Y.; Marotzke, J.; Bala, G.; Cao, L.; Corti, S.; Dunne, J.P.; Engelbrecht, F.; Fischer, E.; Fyfe, J.C.; Jones, C.; et al. Future Global Climate: Scenario-Based Projections and Near-Term Information. In *Climate Change 2021: The Physical Science Basis. Contribution of Working Group I to the Sixth Assessment Report of the Intergovernmental Panel on Climate Change*; Masson-Delmotte, V., Zhai, P., Pirani, A., Connors, S.L., Péan, C., Berger, S., Caud, N., Chen, Y., Goldfarb, L., Gomis, M.I., et al., Eds.; Cambridge University Press: Cambridge, UK; New York, NY, USA, 2021; pp. 553–672. [CrossRef]
65. Hegerl, G.; Black, E.; Allan, R.P.; Ingram, W.J.; Polson, D.; Trenberth, K.E.; Chadwick, R.S.; Arkin, P.A.; Sarojini, B.B.; Becker, A.; et al. Challenges in quantifying changes in the global water cycle. *Bull. Am. Meteorol. Soc.* **2015**, *96*, 1097–1115. [CrossRef]
66. Josey, S.A.; Somot, S.; Tsimplis, M. Impacts Of Atmospheric Modes Of Variability On Mediterranean Sea Surface Heat Exchange. *J. Geophys. Res.—Oceans* **2011**, *116*, C02032. [CrossRef]